

Equation of State for the Lennard-Jones Fluid ^{EP}

Cite as: J. Phys. Chem. Ref. Data **45**, 023101 (2016); <https://doi.org/10.1063/1.4945000>

Submitted: 25 January 2016 • Accepted: 16 March 2016 • Published Online: 06 May 2016

Monika Thol, Gabor Rutkai, Andreas Köster, et al.

COLLECTIONS

^{EP} This paper was selected as an Editor's Pick



View Online



Export Citation



CrossMark

ARTICLES YOU MAY BE INTERESTED IN

Phase diagrams of Lennard-Jones fluids

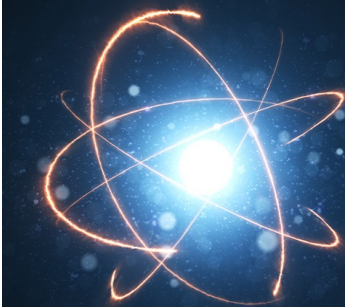
The Journal of Chemical Physics **96**, 8639 (1992); <https://doi.org/10.1063/1.462271>

Phase diagram and universality of the Lennard-Jones gas-liquid system

The Journal of Chemical Physics **136**, 204102 (2012); <https://doi.org/10.1063/1.4720089>

An EOS for the Lennard-Jones fluid: A virial expansion approach

AIP Advances **9**, 125206 (2019); <https://doi.org/10.1063/1.5119761>



Journal of Physical and
Chemical Reference Data

READ TODAY!

CODATA Recommended Values of the
Fundamental Physical Constants: 2018

Equation of State for the Lennard-Jones Fluid

Monika Thol^{a)}

Lehrstuhl für Thermodynamik, Ruhr-Universität Bochum, Universitätsstraße 150, 44801 Bochum, Germany

Gabor Rutkai and Andreas Köster

Lehrstuhl für Thermodynamik und Energietechnik, Universität Paderborn, Warburger Straße 100, 33098 Paderborn, Germany

Rolf Lustig

Department of Chemical and Biomedical Engineering, Cleveland State University, Cleveland, Ohio 44115, USA

Roland Span

Lehrstuhl für Thermodynamik, Ruhr-Universität Bochum, Universitätsstraße 150, 44801 Bochum, Germany

Jadran Vrabec

Lehrstuhl für Thermodynamik und Energietechnik, Universität Paderborn, Warburger Straße 100, 33098 Paderborn, Germany

(Received 25 January 2016; accepted 16 March 2016; published online 6 May 2016)

An empirical equation of state correlation is proposed for the Lennard-Jones model fluid. The equation in terms of the Helmholtz energy is based on a large molecular simulation data set and thermal virial coefficients. The underlying data set consists of directly simulated residual Helmholtz energy derivatives with respect to temperature and density in the canonical ensemble. Using these data introduces a new methodology for developing equations of state from molecular simulation. The correlation is valid for temperatures $0.5 < T/T_c < 7$ and pressures up to $p/p_c = 500$. Extensive comparisons to simulation data from the literature are made. The accuracy and extrapolation behavior are better than for existing equations of state. © 2016 AIP Publishing LLC for the National Institute of Standards and Technology. [<http://dx.doi.org/10.1063/1.4945000>]

Key words: equation of state; Helmholtz energy; Lennard-Jones model fluid; molecular simulation; thermodynamic properties.

CONTENTS

1. Introduction	2
2. Equation of State	3
3. Molecular Simulation	3
4. Equations of State from the Literature	5
5. New Equation of State	8
5.1. Helmholtz energy derivatives	8
5.2. Thermal virial coefficients	15
5.3. Vapor–liquid equilibrium	17
5.4. Density at homogeneous states	21
5.5. Critical point	26
5.6. Caloric properties	27
5.7. Physical behavior and extrapolation	31
6. Conclusion	34

Acknowledgments	35
7. References	35

List of Tables

1. Definitions of common thermodynamic properties and their relation to the Helmholtz energy	3
2. Parameters of the residual part of the present equation of state	5
3. Equations of state for the Lennard-Jones fluid from the literature	5
4. Average absolute relative deviations (AAD) of the data bases of five selected equations of state from the literature	6
5. Average absolute relative deviations (AAD) of the present equation of state and the most prominent equations from the literature based on the simulation data of this work.	10

^{a)}Electronic mail: M.Thol@thermo.ruhr-uni-bochum.de.
© 2016 AIP Publishing LLC.

6.	Selected points on the characteristic ideal curves calculated with the present equation of state	16	13.	First derivative of the second and third thermal virial coefficients with respect to temperature.	16
7.	Parameters of the ancillary equations for vapor pressure, saturated liquid density, and saturated vapor density	18	14.	Relative deviation of literature data for vapor pressure, saturated liquid density, and saturated vapor density from the present equation of state.	17
8.	Average absolute relative deviations of vapor pressure, saturated liquid density, and saturated vapor density from literature data relative to the present equation of state	18	15.	Representation of vapor-phase density data.	21
9.	Average absolute relative deviations of simulation data in homogeneous states from the literature relative to the present equation of state.	19	16.	Representation of liquid-phase density data.	22
10.	Critical parameters of the Lennard-Jones fluid from the literature	25	17.	Representation of density in the supercritical region.	23
			18.	Representation of literature data for pressure in the critical region.	24
			19.	Comparison of metastable gaseous pressure data.	24
			20.	Selected critical parameters from the literature.	26
			21.	Relative deviation of literature data for residual internal energy from the present equation of state.	27
			22.	Relative deviation of literature data for isochoric heat capacity from the present equation of state.	28
			23.	Isochoric heat capacity versus temperature.	28
			24.	Relative deviation of literature data for isobaric heat capacity from the present equation of state.	29
			25.	Isobaric heat capacity versus temperature along isobars.	29
			26.	Comparison of literature data for the Grüneisen coefficient with the present equation of state.	30
			27.	Relative deviation of literature data for speed of sound from the present equation of state.	30
			28.	Comparison of literature data for the Joule–Thomson coefficient with the present equation of state.	31
			29.	Relative deviation of literature data for thermal expansion coefficient α , isothermal compressibility β_T , and thermal pressure coefficient γ from the present equation of state.	32
			30.	Residual isochoric heat capacity and speed of sound versus temperature along isobars.	33
			31.	Temperature versus density along isobars.	33
			32.	Characteristic ideal curves as defined by Span and Wagner. ¹²²	33
			33.	Grüneisen coefficient versus density along isotherms (top) and Grüneisen coefficient versus temperature (bottom) along isobars.	34
			34.	Phase identification parameter versus density along isotherms (top) and versus temperature along isobars (bottom).	34

List of Figures

1.	Third virial coefficient versus temperature from the literature.	5
2.	Extrapolation behavior of five equations of state from the literature along the isotherm $T = 10$	7
3.	Comparison of five equations of state from the literature with the corresponding data sets used for their development.	8
4.	Data set used to develop the present equation of state.	9
5.	Relative deviation of simulated residual Helmholtz energy A_{00}^r data (circles) from the present equation of state.	11
6.	Relative deviation of simulated first derivative of the residual Helmholtz energy with respect to density A_{01}^r data (circles) from the present equation of state.	12
7.	Relative deviation of simulated first derivative of the residual Helmholtz energy with respect to inverse temperature A_{10}^r data (circles) from the present equation of state.	12
8.	Relative deviation of simulated second derivative of the residual Helmholtz energy with respect to density A_{02}^r data (circles) from the present equation of state.	13
9.	Relative deviation of simulated second derivative of the residual Helmholtz energy with respect to inverse temperature A_{20}^r data (circles) from the present equation of state.	13
10.	Relative deviation of simulated mixed derivative of the residual Helmholtz energy with respect to density and inverse temperature A_{11}^r data (circles) from the present equation of state.	14
11.	Relative deviation of the simulated third derivatives of the residual Helmholtz energy with respect to density and inverse temperature data (circles) from the present equation of state.	14
12.	Second, third, and fourth thermal virial coefficients.	15

1. Introduction

The Lennard-Jones 12–6 (LJ) model is the most widely used intermolecular interaction potential in simulation history that is sufficiently realistic to represent small spherical and nonpolar molecules.^{1,2} It was studied extensively in the last decades, concluding that it may serve as an important model for studying phase equilibria, phase change processes, clustering behavior, or transport and interface properties of simple fluids. It is commonly expressed as

$$u_{\text{LJ}} = 4\varepsilon \left[\left(\frac{\sigma}{r} \right)^{12} - \left(\frac{\sigma}{r} \right)^6 \right], \quad (1)$$

where σ and ε are size and energy parameters, and r is the distance between two particles.

Although molecular simulation has evolved to a significant contribution in science and engineering, the generation of fluid property data sets is still a challenge. For practical purposes, thermodynamic data must be rationalized in the form of robust correlations. In particular, fundamental equation of state (EOS) correlations allow for the computation of any thermodynamic property given as combinations of derivatives with respect to its natural variables. Here, we use the Massieu–Planck potential $F(N, V, 1/T)/(k_{\text{B}}T)$ with Helmholtz energy F , temperature T , volume V , number of particles N , and Boltzmann constant k_{B} .

A number of EOS for the LJ fluid exist in the literature. The latest and most accurate ones are Johnson *et al.*,³ Kolafa and Nezbeda,⁴ and Mecke *et al.*,⁵ which were set up on the basis of pressure and internal energy data from molecular simulation. As opposed to those previous attempts, the underlying data set for the present EOS consists only of direct derivatives of the residual Helmholtz energy. Preliminary results for such a new approach were presented by Rutkai *et al.*⁶ Using residual Helmholtz energy derivatives instead of common thermodynamic properties in thermodynamic correlations was first introduced 20 years ago. Lustig presented a series of statistical thermodynamic developments,^{7–13} which were successfully employed by other researchers.^{14–16} Recently, the methodology was extended to the canonical ensemble.^{17,18} The outline in Ref. 18 is the basis of this work.

2. Equation of State

In this section, a new equation of state for the Lennard-Jones model fluid in terms of the reduced Helmholtz energy is presented. All relevant variables together with the mathematical expressions of how to calculate thermodynamic properties are given.

The size and energy parameters σ and ε of the potential were used to reduce all properties to dimensionless numbers of order unity, e.g., temperature $T^* = k_{\text{B}}T/\varepsilon$, density $\rho^* = \rho\sigma^3$ (with $\rho = v^{-1} = N/V$), or pressure $p^* = p\sigma^3/\varepsilon$. For brevity, asterisks are omitted in the following, although reduced quantities are used throughout.

The equation of state is written in terms of the reduced Helmholtz energy α as a function of inverse temperature and density. Separate terms denote ideal-gas behavior (superscript o) and residual contribution (superscript r)

$$\alpha(\tau, \delta) = \frac{a^{\text{o}}(T, \rho) + a^{\text{r}}(T, \rho)}{k_{\text{B}}T} = \alpha^{\text{o}}(\tau, \delta) + \alpha^{\text{r}}(\tau, \delta), \quad (2)$$

with $a = F/N$ the Helmholtz energy per particle, $\tau = T_{\text{c}}/T$, and $\delta = \rho/\rho_{\text{c}}$. For the critical properties, $T_{\text{c}} = 1.32$ and $\rho_{\text{c}} = 0.31$ are used. Detailed information on the determination of the critical parameters is given in Section 5.5.

α^{o} relates to a hypothetical ideal gas. α^{r} represents the residual Helmholtz energy under full intermolecular interactions in the fluid. All thermodynamic properties can be calculated from

Eq. (2) and its derivatives with respect to τ and δ . For these derivatives, the following notation is used:

$$A_{mn} = A_{mn}^{\text{o}} + A_{mn}^{\text{r}} = \tau^m \delta^n \frac{\partial^{m+n} (\alpha^{\text{o}} + \alpha^{\text{r}})}{\partial \tau^m \partial \delta^n}. \quad (3)$$

Thermodynamic properties used in this work are related in Table 1.

As a classical monatomic model, the isobaric heat capacity of the ideal gas is $c_p^{\text{o}}/k_{\text{B}} = 2.5$. Integration yields

$$\alpha^{\text{o}} = \ln \delta + 1.5 \ln \tau + c_1 \tau + c_2. \quad (40)$$

The values $c_1 = -1.515\,151\,515$ and $c_2 = 6.262\,265\,814$ yield $h_0^{\text{o}} = 0$ and $s_0^{\text{o}} = 0$ at $T_0 = 0.8$, $p_0 = 0.001$, and the corresponding density of the ideal gas $\rho_0 = p_0/T_0$.

The correlation of this work consists of 6 polynomial, 6 exponential, and 11 Gaussian bell-shaped terms

$$\begin{aligned} \alpha^{\text{r}}(\tau, \delta) = & \sum_{i=1}^6 n_i \delta^{d_i} \tau^{t_i} + \sum_{i=7}^{12} n_i \delta^{d_i} \tau^{t_i} \exp(-\delta^{l_i}) \\ & + \sum_{i=13}^{23} n_i \delta^{d_i} \tau^{t_i} \exp(-\eta_i(\delta - \varepsilon_i)^2 - \beta_i(\tau - \gamma_i)^2). \end{aligned} \quad (41)$$

It is valid for temperatures $0.661 < T < 9$ and for pressures up to $p = 65$, corresponding to $0.5 < T/T_{\text{c}} < 7$ and $p/p_{\text{c}} = 500$. The adjustable parameters (coefficients n_i , temperature exponents t_i , and Gaussian bell-shaped parameters) as well as the density exponents d_i , are listed in Table 2.

3. Molecular Simulation

In this section, the main information for the molecular simulation of thermodynamic properties is provided. The new approach of direct simulations of reduced Helmholtz derivatives is discussed.

When setting up fundamental equations of state on the basis of experimental data, not every individual derivative with respect to its independent variables can be employed. The development of an EOS explicit in $F/(k_{\text{B}}T)$ would ideally require the reduced Helmholtz energy itself and its derivatives with respect to the inverse temperature and the density. With experimentally accessible thermodynamic properties, only derivatives A_{01}^{r} and A_{20}^{r} can be computed individually. A_{11}^{r} and A_{02}^{r} are nonlinearly related to speed of sound and heat capacities.⁶ Fitting Helmholtz energy derivatives directly does not require linearization of any thermodynamic property. Consequently, the fitting procedure allows for an explicit study of all derivatives of the fundamental equation of state.

As molecular simulation allows for the calculation of the residual Helmholtz energy itself, an EOS could be developed considering A_{00}^{r} simulation data only, at least in principle. However, an extremely dense and equally distributed grid of state points would have to be sampled across the entire fluid region to capture subtle features of the Helmholtz energy surface. Data sets for fitting EOS should thus contain as much independent thermodynamic information as possible. At present, efficient generation of extensive data sets is cumbersome because most molecular simulation software tools are restricted to

TABLE 1. Definitions of common thermodynamic properties and their relation to the Helmholtz energy

Property	Reduced quantity Relation to the reduced Helmholtz energy		
<i>Pressure</i>	$p = -(\partial a / \partial v)_T \quad (4)$	$p / (\rho RT) = (1 + A_{01}^r) \quad (5)$	
<i>Derivatives of pressure with respect to</i>			
Density	$(\partial p / \partial \rho)_T \quad (6)$	$(\partial p / \partial \rho)_T = T (1 + 2A_{01}^r + A_{02}^r) \quad (7)$	
Temperature	$(\partial p / \partial T)_\rho \quad (8)$	$(\partial p / \partial T)_\rho = \rho (1 + A_{01}^r - A_{11}^r) \quad (9)$	
<i>Entropy</i>	$s = -(\partial a / \partial T)_v \quad (10)$	$s = A_{10}^o + A_{10}^r - A_{00}^o - A_{00}^r \quad (11)$	
<i>Internal energy</i>	$u = a + T s \quad (12)$	$u / T = A_{10}^o + A_{10}^r \quad (13)$	
<i>Enthalpy</i>	$h = u + p v \quad (14)$	$h / T = 1 + A_{10}^o + A_{10}^r + A_{01}^r \quad (15)$	
<i>Isochoric heat capacity</i>	$c_v = (\partial u / \partial T)_v \quad (16)$	$c_v = -(A_{20}^o + A_{20}^r) \quad (17)$	
<i>Isobaric heat capacity</i>	$c_p = (\partial h / \partial T)_p \quad (18)$	$c_p = -(A_{20}^o + A_{20}^r) + \frac{(1 + A_{01}^r - A_{11}^r)^2}{1 + 2A_{01}^r + A_{02}^r} \quad (19)$	
<i>Gibbs energy</i>	$g = h - T s \quad (20)$	$g / T = 1 + A_{00}^o + A_{00}^r + A_{01}^r \quad (21)$	
<i>Speed of sound</i>	$w = \sqrt{(\partial p / \partial \rho)_s} \quad (22)$	$w^2 / T = 1 + 2A_{01}^r + A_{02}^r - \frac{(1 + A_{01}^r - A_{11}^r)^2}{A_{20}^o + A_{20}^r} \quad (23)$	
<i>Grüneisen coefficient</i>	$\Gamma = \frac{(\partial p / \partial T)_\rho}{\rho c_v} \quad (24)$	$\Gamma = \frac{1 + A_{01}^r - A_{11}^r}{-(A_{20}^o + A_{20}^r)} \quad (25)$	
<i>Phase identification parameter</i>	$\Pi = 2 - \left(\frac{\partial^2 p / \partial \rho \partial T}{(\partial p / \partial T)_\rho} - \frac{(\partial^2 p / \partial \rho^2)_T}{(\partial p / \partial \rho)_T} \right) \rho \quad (26)$	$\Pi = 2 - \frac{1 + 2A_{01}^r + A_{02}^r - A_{11}^r - A_{12}^r}{1 + A_{01}^r - A_{11}^r} + \frac{2A_{01}^r + 4A_{02}^r + A_{03}^r}{1 + 2A_{01}^r + A_{02}^r} \quad (27)$	
<i>2nd thermal virial coefficient</i>	$B = \lim_{\rho \rightarrow 0} (\partial (p / (\rho RT)) / \partial \rho)_T \quad (28)$	$B\rho = \lim_{\delta \rightarrow 0} (A_{01}^r / \delta) \quad (29)$	
<i>3rd thermal virial coefficient</i>	$C = \frac{1}{2} \lim_{\rho \rightarrow 0} (\partial^2 (p / (\rho RT)) / \partial \rho^2)_T \quad (30)$	$C\rho^2 = \lim_{\delta \rightarrow 0} (A_{02}^r / \delta^2) \quad (31)$	
<i>4th thermal virial coefficient</i>	$D = \frac{1}{6} \lim_{\rho \rightarrow 0} (\partial^3 (p / (\rho RT)) / \partial \rho^3)_T \quad (32)$	$D2\rho^3 = \lim_{\delta \rightarrow 0} (A_{03}^r / \delta^3) \quad (33)$	
<i>Isothermal compressibility</i>	$\beta_T = 1 / (\rho (\partial p / \partial \rho)_T) \quad (34)$	$\beta_T = \rho^{-1} T (1 + 2A_{01}^r + A_{02}^r) \quad (35)$	
<i>Thermal pressure coefficient</i>	$\gamma = (\partial p / \partial T)_\rho \quad (36)$	$\gamma = \rho (1 + A_{01}^r - A_{11}^r) \quad (37)$	
<i>Thermal expansion coefficient</i>	$\alpha = \beta_T \gamma = \frac{(\partial p / \partial T)_\rho}{\rho (\partial p / \partial \rho)_T} \quad (38)$	$\alpha = (1 + A_{01}^r - A_{11}^r) / (T (1 + 2A_{01}^r + A_{02}^r)) \quad (39)$	

TABLE 2. Parameters of the residual part of the present equation of state according to Eq. (41)

i	n_i	t_i	d_i	l_i	η_i	β_i	γ_i	ε_i
1	$0.520\,807\,30 \times 10^{-2}$	1.000	4	—				
2	$0.218\,625\,20 \times 10^{+1}$	0.320	1	—				
3	$-0.216\,101\,60 \times 10^{+1}$	0.505	1	—				
4	$0.145\,270\,00 \times 10^{+1}$	0.672	2	—				
5	$-0.204\,179\,20 \times 10^{+1}$	0.843	2	—				
6	$0.186\,952\,86 \times 10^0$	0.898	3	—				
7	$-0.909\,884\,45 \times 10^{-1}$	1.294	5	1				
8	$-0.497\,456\,10 \times 10^0$	2.590	2	2				
9	$0.109\,014\,31 \times 10^0$	1.786	2	1				
10	$-0.800\,559\,22 \times 10^0$	2.770	3	2				
11	$-0.568\,839\,00 \times 10^0$	1.786	1	2				
12	$-0.620\,862\,50 \times 10^0$	1.205	1	1				
13	$-0.146\,671\,77 \times 10^{+1}$	2.830	1	—	2.067	0.625	0.710	0.2053
14	$0.189\,146\,90 \times 10^{+1}$	2.548	1	—	1.522	0.638	0.860	0.4090
15	$-0.138\,370\,10 \times 10^0$	4.650	2	—	8.820	3.910	1.940	0.6000
16	$-0.386\,964\,50 \times 10^0$	1.385	3	—	1.722	0.156	1.480	1.2030
17	$0.126\,570\,20 \times 10^0$	1.460	3	—	0.679	0.157	1.490	1.8290
18	$0.605\,781\,00 \times 10^0$	1.351	2	—	1.883	0.153	1.945	1.3970
19	$0.117\,918\,90 \times 10^{+1}$	0.660	1	—	3.925	1.160	3.020	1.3900
20	$-0.477\,326\,79 \times 10^0$	1.496	2	—	2.461	1.730	1.110	0.5390
21	$-0.992\,185\,75 \times 10^{+1}$	1.830	3	—	28.20	383.0	1.170	0.9340
22	$-0.574\,793\,20 \times 10^0$	1.616	1	—	0.753	0.112	1.330	2.3690
23	$0.377\,292\,30 \times 10^{-2}$	4.970	1	—	0.820	0.119	0.240	2.4300

very few thermodynamic properties, such as internal energy, pressure, isochoric, or isobaric heat capacities. Here, we apply the methodology of Lustig.^{17,18} Any A_{mn}^r is simultaneously available from one single NVT ensemble simulation for a given state point. The approach was implemented in the molecular simulation tool *ms2* (Ref. 19) up to order $m = 3$ and $n = 2$: A_{01}^r , A_{10}^r , A_{02}^r , A_{20}^r , A_{11}^r , A_{12}^r , A_{21}^r , and A_{30}^r . Additionally, A_{00}^r can be determined using a rigorous test-particle insertion method.²⁰

The underlying simulation data set was generated by sampling about 200 state points with the simulation tool *ms2*,¹⁹ covering the homogenous fluid region $0.7 < T < 9$, $\rho < 1.08$ and pressures up to $p = 65$. At each state point, 1372 LJ particles were equilibrated and then sampled for 10^6 cycles with Monte Carlo NVT ensemble simulations,²¹ measuring the derivatives mentioned above.

4. Equations of State from the Literature

In this section, the prominent and recent equations for the Lennard-Jones fluid are discussed. The quality of those equations is analyzed by comparing to the underlying simulation data sets and the extrapolation behavior.

TABLE 3. Equations of state for the Lennard-Jones fluid from the literature

Authors	Year	EOS type	Critical parameters		Range of validity	
			T_c	ρ_c	T	ρ
Nicolas <i>et al.</i> ²⁵	1979	MBWR	1.35	0.35	0.55–6	≤ 1.2
Johnson <i>et al.</i> ³	1993	MBWR	1.313	0.31	0.7–6	≤ 1.25
Kolafa and Nezbeda ⁴	1994	MBWR	1.3396	0.3108	0.7–20	≤ 1.2
Mecke <i>et al.</i> ⁵	1996	α + HS term	1.328	0.3107	0.7–10 ^a	≤ 1.2
May and Mausbach ³⁰	2012	MBWR	1.3145	0.316	0.5–6	≤ 1.2

^aReasonable extrapolation behavior up to $T = 100$ for $\rho \leq 1$.

For the Lennard-Jones fluid, many equations of state are available in the literature. Until the early 1990s, there were only semitheoretical, e.g., of Levesque and Verlet,²² McDonald and Singer,²³ or Song and Mason,²⁴ and empirical equations using the modified Benedict–Webb–Rubin (MBWR) form, e.g., Nicolas *et al.*,²⁵ Adachi *et al.*,²⁶ or Miyano.²⁷ The semitheoretical equations are mostly restricted to a small range of validity. They have few adjustable parameters so that they are not flexible enough to represent all thermodynamic data within their estimated statistical uncertainty over the entire fluid range. The equations expressed in the MBWR form are more flexible due to the large number of adjustable parameters. Thus, the entire fluid range can be modeled more accurately than with

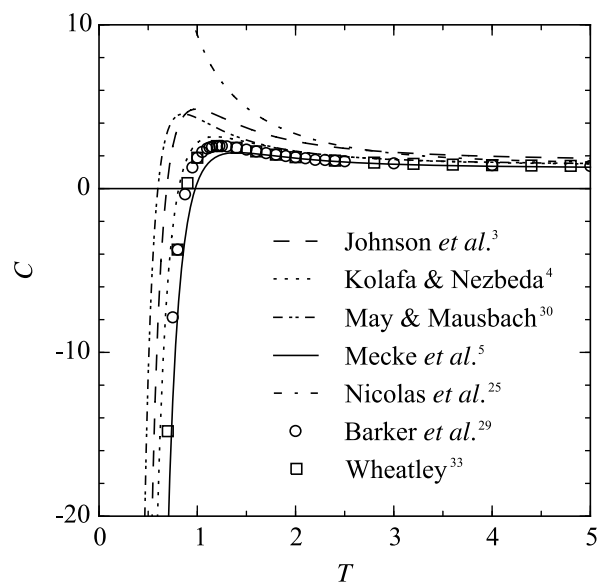


Fig. 1. Third virial coefficient versus temperature from the literature.

semithoretical equations. However, lacking physical background, their extrapolation behavior has to be investigated carefully. For the calculation of any thermodynamic property, the pressure-explicit MBWR form must be integrated to yield the Helmholtz energy.²⁸ The first fundamental equations of state for the Lennard-Jones fluid in terms of the Helmholtz energy were published by Kolafa and Nezbeda⁴ and Mecke *et al.*⁵

Table 3 lists prominent and recent equations for the Lennard-Jones fluid. The most cited equation is Johnson *et al.*,³ so it will be discussed in more detail here. Based on the MBWR equation of Nicolas *et al.*,²⁵ it consists of 32 linear parameters and one nonlinear parameter. The first five parameters were fitted to

second virial coefficient data of Barker *et al.*,²⁹ which are exact. All other parameters were established by fitting to pressure and internal energy data sampled with molecular dynamics simulation. No VLE data were used, but a critical point at $T_c = 1.313$ and $\rho_c = 0.31$ was applied. Unlike Nicolas *et al.*,²⁵ the equation of Johnson *et al.*³ also follows the trend of the third virial coefficient of Barker *et al.*²⁹ (see Fig. 1). Although they assumed a better representation of the vapor-liquid equilibrium as a consequence, the third virial coefficient was overestimated systematically.

To date, the most accurate equation of state for the Lennard-Jones fluid is the one published by Mecke *et al.*⁵ The correla-

TABLE 4. Average absolute relative deviations (AAD) of the data bases of five selected equations of state from the literature. Here, only the data points that are located in the homogenous fluid region are considered. For the determination of the vapor-liquid equilibrium, all equations were applied. Data located in the solid-liquid two-phase region according to Ahmed and Sadus³⁴ were not considered. The best AAD for each data set among the previous EOS is written in bold face

	No. of pts.	Nicolas <i>et al.</i> ²⁵	Johnson <i>et al.</i> ³	Kolafa and Nezbeda ⁴	Mecke <i>et al.</i> ⁵	May and Mausbach ³⁰	This work
<i>ppT</i> data							
Adams ^{35 a}	12	2.360	1.970	2.076	2.004	2.024	1.990
Adams ^{36 a}	15	0.423	0.721	0.731	0.760	0.538	0.740
Hansen ^{37 a}	6	0.320	0.232	0.208	0.164	0.205	0.167
Hansen and Verlet ^{38 a}	7	1.252	0.862	0.783	0.766	0.872	0.798
Johnson <i>et al.</i> ^{3 b,c,d}	149	0.690	0.247	0.151	0.109	0.196	0.129
Kolafa <i>et al.</i> ^{39 d}	37	0.760	0.458	0.222	0.187	0.375	0.244
Kolafa and Nezbeda ^{4 b,d}	9	1.560	1.162	0.374	0.236	0.906	0.317
Levesque and Verlet ^{22 a}	17	52.55	48.20	49.14	49.40	48.41	48.88
McDonald and Singer ^{23 a}	43	0.362	0.433	0.376	0.406	0.377	0.401
Mecke <i>et al.</i> ^{5 b}	5	8.205	2.374	0.352	0.522	2.274	1.435
Meier ^{14 e}	287	0.952	0.353	0.128	0.087	0.206	0.120
Miyano ^{27 b}	63	1.722	4.236	3.104	1.660	3.687	1.532
Nicolas <i>et al.</i> ^{25 a,b}	55	0.551	0.709	0.533	0.518	0.661	0.542
Saager and Fischer ^{40 b}	25	0.568	0.143	0.131	0.120	0.231	0.122
Verlet ^{41 a}	32	3.896	3.158	2.926	2.908	3.096	2.981
<i>u^r</i> data							
Adams ^{35 a}	12	1.965	2.026	1.932	1.731	1.880	1.710
Adams ^{36 a}	15	0.398	0.733	0.670	0.648	1.118	0.652
Hansen ^{37 a}	6	0.637	0.801	0.857	0.620	0.589	0.567
Johnson <i>et al.</i> ^{3 b,c,d}	149	1.497	1.129	1.333	0.305	0.933	0.392
Kolafa <i>et al.</i> ^{39 d}	37	1.082	0.459	0.360	0.203	0.696	0.166
Kolafa and Nezbeda ^{4 d}	9	4.416	10.15	11.05	0.325	8.617	0.549
Levesque and Verlet ^{22 a}	32	0.862	1.113	1.105	1.031	1.110	0.785
McDonald and Singer ^{23 a}	43	0.302	0.426	0.417	0.380	0.592	0.377
Mecke <i>et al.</i> ^{5 b}	5	3.346	0.478	0.521	0.856	1.458	0.752
Meier ^{14 e}	287	1.860	0.864	0.988	0.198	0.646	0.205
Miyano ^{27 b}	63	27.07	42.76	43.09	4.469	39.84	3.811
Nicolas <i>et al.</i> ^{25 a,b}	55	0.857	1.569	1.700	0.684	1.783	0.826
Saager and Fischer ^{40 b}	25	0.278	0.581	0.619	0.160	0.710	0.221
Verlet ^{41 a}	32	0.772	0.980	0.933	0.799	1.051	0.730

^aUsed by Nicolas *et al.*;²⁵ additionally, data of Barker *et al.*²⁹ (*B*) were applied to the fit.

^bUsed by Mecke *et al.*;⁵ additionally, data of Barker *et al.*²⁹ (*B*, *C*), Kriebel (numerical values not available in the literature), and Lotfi *et al.*⁴² (*ppT*) were applied to the fit.

^cUsed by Johnson *et al.*;³ additionally, data of Barker *et al.*²⁹ (*B*, *C*) were used for comparison.

^dUsed by Kolafa and Nezbeda;⁴ additionally, data of Barker *et al.*²⁹ (*B*) and Lotfi *et al.*⁴² (*ppT*) were applied to the fit.

^eUsed by May and Mausbach.³⁰

tion is given in the reduced Helmholtz energy α augmented by a hard-body term. A linear structural optimization algorithm introduced by Setzmann and Wagner³¹ was used. The data set consisted of pressure, residual internal energy, virial coefficients, and VLE data, and the equation is valid for $0.7 \leq T \leq 10$ and $\rho \leq 1.2$. The critical temperature $T_c = 1.328$ was taken from Valleau³² as a constraint, and the critical density $\rho_c = 0.3107$ was obtained from a linear extrapolation of the rectilinear diameter. The authors stated that the extrapolation behavior was correct up to $T = 100$. Third virial coefficient data at low temperatures are also best reproduced as illustrated in Fig. 1. The equations of Kolafa and Nezbeda,⁴ Johnson *et al.*,³ and May and Mausbach³⁰ follow the course of the third virial coefficient, but deviate systematically.

For an assessment of the equation of state correlations listed in Table 3, the data sets that were the basis for the development of these equations are compared to each of them. Based on those results, only the most reliable EOS will be considered for comparison in the following.

Some statistical definitions are used for the evaluation of the equations. The relative deviation of a given property X is defined as

$$\Delta X = 100 \frac{X_{\text{DATA}} - X_{\text{EOS}}}{X_{\text{DATA}}}, \quad (42)$$

and the average absolute relative deviation AAD is

$$\text{AAD} = \frac{1}{N} \sum_{i=1}^N |\Delta X_i|. \quad (43)$$

In this work, the average absolute relative deviation is separated into different temperature and pressure ranges to avoid misleading results caused by certain regions, e.g., the critical region. The homogeneous fluid range is separated into the gas and liquid phases, and into the critical and supercritical regions. The critical region is defined by $0.98 \leq T/T_c \leq 1.1$ and $0.7 \leq \rho/\rho_c \leq 1.4$. The supercritical region is furthermore divided into three areas: the region of low densities (LD: $\rho/\rho_c < 0.6$), of medium densities (MD: $0.6 \leq \rho/\rho_c \leq 1.5$), and of high densities (HD: $\rho/\rho_c > 1.5$). The vapor-liquid equilibrium data are split into three different temperature ranges: the region of low temperatures (LT: $T/T_c < 0.6$), of medium temperatures (MT: $0.6 \leq T/T_c \leq 0.98$), and of high temperatures (HT: $T/T_c > 0.98$).

In Table 4, the average absolute relative deviation of each publication calculated with the five selected equations of state is listed. In this table, only homogeneous fluid states are considered. It is obvious that the EOS of Mecke *et al.*⁵ is the most accurate with respect to the $p\rho T$ data as well as the residual internal energy. Especially for the most comprehensive data sets, e.g., Meier,¹⁴ Johnson *et al.*,³ Miyano,²⁷ Nicolas *et al.*,²⁵ and Saager and Fischer,⁴⁰ the best representation is given by Mecke *et al.*⁵ The reason for the large difference between the AAD of the internal energy data of Miyano²⁷ calculated from the equation of Mecke *et al.*⁵ and all other equations is a different extrapolation behavior, which is illustrated in Fig. 2. There, the course of the isotherm $T = 10$ is presented for very high densities. Although the investigated region is located deeply in the solid phase, a wrong extrapolation behavior also

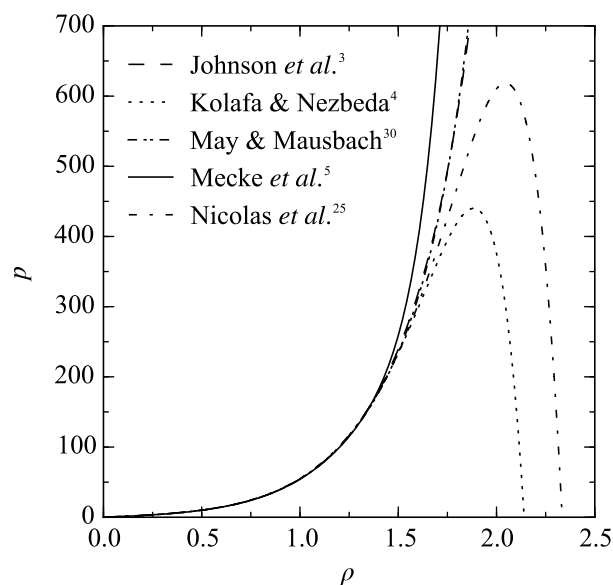


Fig. 2. Extrapolation behavior of five equations of state from the literature along the isotherm $T = 10$.

causes a wrong shape of the isotherm in the fluid region.⁴³ The EOS of Mecke *et al.*⁵ is suitable under extreme conditions of temperature, pressure, and density, whereas the other equations exhibit deficiencies. The qualitative behavior of the equations of Johnson *et al.*³ and May and Mausbach³⁰ is reasonable because no negative pressures occur. The negative pressures calculated by Nicolas *et al.*²⁵ and Kolafa and Nezbeda⁴ are probably caused by a negative coefficient of a polynomial term or a low-order exponential term that is of leading importance in this region.

In Fig. 3, an overview of the deviations of the data sets investigated in Table 4 is given. Deviations in density are shown on the left side, and deviations in internal energy on the right side. Density deviations in the range of $0.2 < \rho < 0.7$ exemplify problems for all but the equation of Mecke *et al.*⁵ The low-density region is described well by Mecke *et al.*⁵ and Kolafa and Nezbeda.⁴ The simulation data of Miyano²⁷ at $\rho = 1$ detect deficiencies of all equations ($\text{AAD} = 1.72\% - 4.24\%$) whereas Mecke *et al.*⁵ yield $\text{AAD} = 1.66\%$. For the residual internal energy, it is striking that the data set of Meier¹⁴ is by far better reproduced by Mecke *et al.*⁵ ($\text{AAD} = 0.20\%$) than all other correlations ($\text{AAD} = 0.6\% - 1.8\%$). The same follows from the simulation data set of Johnson *et al.*,³ although their EOS was exclusively fitted to those data. The data set of Nicolas *et al.*²⁵ is reproduced best with the equation of Mecke *et al.*⁵ ($\text{AAD} = 0.64\%$). The corresponding EOS²⁵ is accurate in this case ($\text{AAD} = 0.86\%$), but reveals significant problems in the low-density region. The equation of May and Mausbach³⁰ is the most consistent for residual internal energy. Most of the data scatter within $2\% - 3\%$, which is still less accurate than the equation of Mecke *et al.*⁵ We showed that in the fluid region the equation of state of Mecke *et al.*⁵ is significantly superior to any other equation of state in the literature. In the following, we compare our results to that EOS.

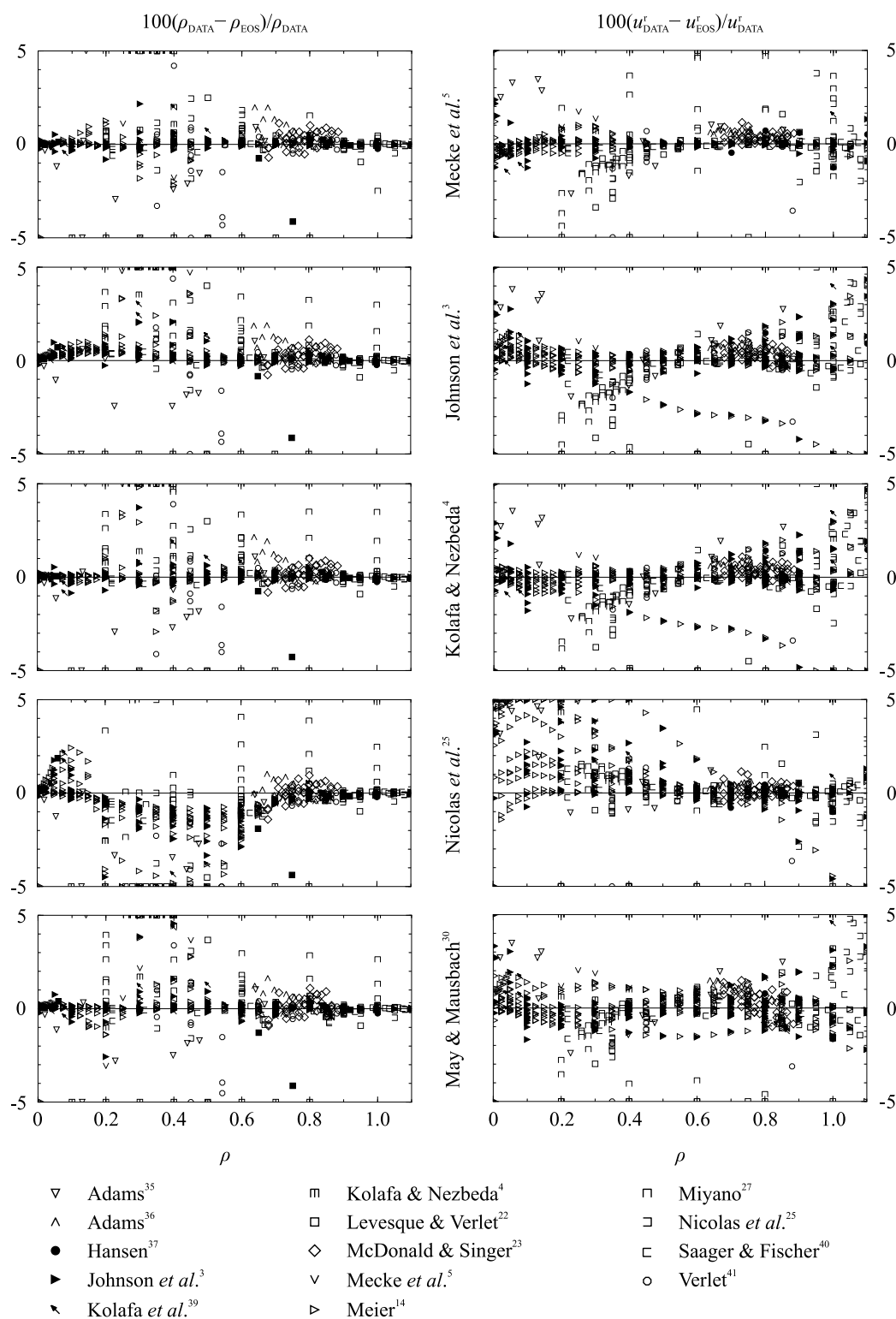


Fig. 3. Comparison of five equations of state from the literature with the corresponding data sets used for their development.

5. New Equation of State

In contrast to the equations examined in Section 4, the new equation is based on derivatives of the residual Helmholtz energy with respect to inverse temperature and density. In the following, the new correlation is compared to previous correlations and previous data sets.

5.1. Helmholtz energy derivatives

The development of the present equation of state for the Lennard-Jones fluid is exclusively based on the simulated reduced residual Helmholtz energy and its derivatives A'_{mn} up to third order, and virial coefficients up to the fourth. No vapor–liquid equilibrium data were considered. The

application of this new data type to a fitting procedure is investigated carefully below. Simulation data exhibit statistical uncertainties, different from experimental uncertainties in the case of real fluids. The use of Helmholtz energy derivatives is the first attempt to apply this strategy in developing an EOS. Among many equations of state for this model available in the literature, the EOS of Mecke *et al.*⁵ was developed by modern fitting techniques and very accurately represents thermal properties as well as the residual internal energy. The goal of the present fundamental EOS is to represent thermal properties with at least such accuracy while improving the representation of caloric properties, other selected thermody-

namic properties, and extrapolation behavior. The new EOS is analyzed in analogy to modern fundamental equations of state for real fluids and is provided in a form that allows for straightforward implementation in common software tools like TREND,⁴⁴ REFPROP,⁴⁵ or CoolProp.⁴⁶

Figure 4 shows simulated state points in the $T - \rho$ plane. The vapor-liquid equilibrium according to the present equation of state and the solid-liquid equilibrium based on the correlations of Ahmed and Sadus³⁴ and van der Hoef⁴⁷ are indicated. At each state point, the residual Helmholtz energy as well as its derivatives with respect to $1/T$ and ρ up to third order (without the third density derivative) were sampled. During the fit,

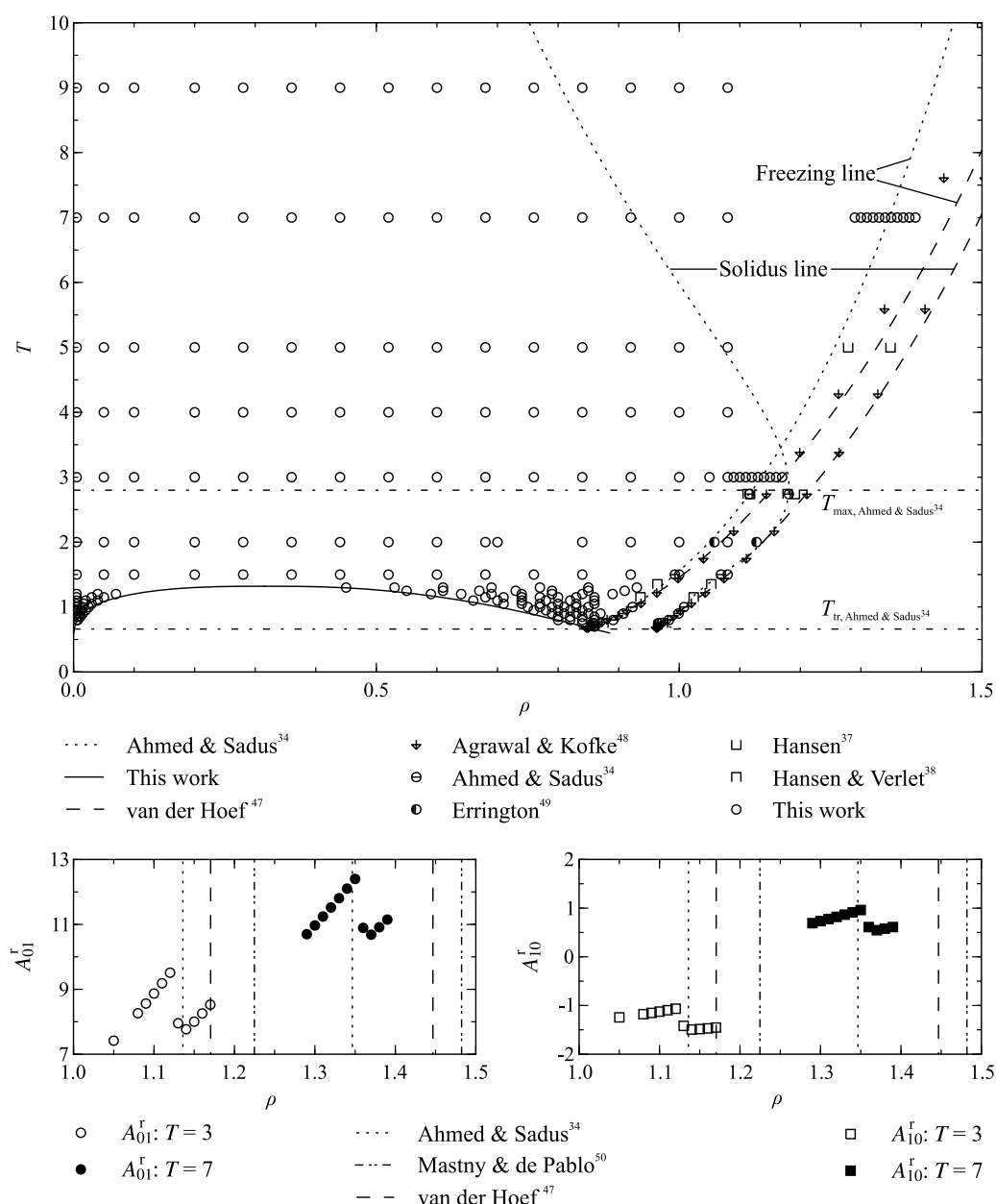


FIG. 4. Top: Data set used to develop the present equation of state. The residual Helmholtz energy and its derivatives up to third order were sampled at each state point. The saturated liquid and vapor lines were calculated with the present equation of state. The solid-liquid equilibrium curves were calculated with the correlations of Ahmed and Sadus³⁴ and van der Hoef⁴⁷. Selected literature data^{34,37,38,48,49} are included for comparison. Bottom: Test simulations of A_{01}^r and A_{10}^r along the isotherms $T = 3$ and $T = 7$ are shown to verify the correlation of Ahmed and Sadus.³⁴ The liquid densities of the solid-liquid equilibrium of Ahmed and Sadus,³⁴ van der Hoef,⁴⁷ and Mastny and de Pablo⁵⁰ are plotted for comparison.

statistical uncertainties served as measures for the reliability of the data. Possible unknown systematic errors were ignored. For temperatures $T > 2.8$, the freezing line of Ahmed and Sadus³⁴ is steeper than that of van der Hoef.⁴⁷ The data of Agrawal and Kofke⁴⁸ and Hansen³⁷ fall in between both correlations. Therefore, test simulations at $T = 3$ and 7 were carried out here for assessment (cf. Fig. 4, bottom). Isothermal jumps in A_{01}^r and A_{10}^r indicate the onset of freezing. The estimated freezing density of Ahmed and Sadus³⁴ is closer to the jump than that of van der Hoef.⁴⁷ Therefore, the correlation of Ahmed and Sadus³⁴ is considered here as a boundary of the liquid phase. The solidus line of Ahmed and Sadus³⁴ is obviously wrong for approximately $T > 2.5$. However, in their publication they

state $T = 2.8$ to be the upper boundary of the range of validity, which is indicated by dashed-dotted lines in Fig. 4, and the unreasonable trend at higher temperatures is an extrapolation effect. Since the present equation of state is explicitly valid in the fluid region only, all available data from the literature beyond that boundary are excluded from the discussion below.

The triple-point temperature $T_{tr} = 0.661$ published by Ahmed and Sadus³⁴ is used as the lower temperature limit of the present equation of state. Other reported triple-point temperatures include Agrawal and Kofke⁴⁸ ($T_{tr} = 0.687 \pm 0.004$), Hansen and Verlet³⁸ ($T_{tr} = 0.68 \pm 0.02$), Johnson *et al.*³ ($T_{tr} = 0.69$), and Ladd and Woodcock⁵¹ ($T_{tr} = 0.67 \pm 0.01$).

TABLE 5. Average absolute relative deviations (AAD) of the present equation of state and the most prominent equations from the literature based on the simulation data of this work (temperature range $T = 0.7$ – 9 , pressure range $p < 65$). No simulation data were generated in the critical region ($0.98 \leq T/T_c \leq 1.1$ and $0.7 \leq \rho/\rho_c \leq 1.4$). Data that are clear outliers for all equations were rejected. The best AAD for each phase and data set is written in bold face

No. of data		Average absolute relative deviations (AAD)/%					
Property		Gas	Liquid	LD ^a	MD ^a	HD ^a	Overall
This work							
A ₀₀ ^r	190	0.10	0.37	0.35	1.40	0.48	0.52
A ₀₁ ^r	190	0.28	0.93	0.52	0.52	0.13	0.53
A ₁₀ ^r	190	0.31	0.02	0.19	0.15	0.12	0.12
A ₀₂ ^r	189	101	5.47	118	3.60	0.70	27.9
A ₂₀ ^r	188	0.43	0.59	0.69	0.84	0.37	0.56
A ₁₁ ^r	187	0.30	0.48	0.29	0.48	1.21	0.63
A ₁₂ ^r	189	105	77.5	126	145	20.4	80.6
A ₂₁ ^r	189	1.78	19.3	3.70	13.9	9.72	12.0
A ₃₀ ^r	183	6.03	3.89	3.63	4.40	2.10	3.70
Mecke <i>et al.</i> ⁵							
A ₀₀ ^r	190	0.07	0.37	0.44	2.85	0.56	0.76
A ₀₁ ^r	190	0.41	1.94	0.73	1.00	0.20	1.01
A ₁₀ ^r	190	0.47	0.01	0.25	0.26	0.13	0.16
A ₀₂ ^r	189	101	5.55	118	3.18	0.69	28.0
A ₂₀ ^r	188	1.07	0.88	1.19	1.63	0.44	0.93
A ₁₁ ^r	187	0.53	0.49	0.25	0.73	1.48	0.77
A ₁₂ ^r	189	115	396	>500	>500	467	>500
A ₂₁ ^r	189	4.00	21.3	3.72	37.3	15.4	18.0
A ₃₀ ^r	183	14.6	6.07	3.87	7.17	2.17	5.97
Kolafa and Nezbeda ⁴							
A ₀₀ ^r	191	0.36	0.39	1.07	0.81	0.77	0.57
A ₀₁ ^r	191	0.22	3.90	0.87	1.23	1.13	1.82
A ₁₀ ^r	191	19.4	0.09	0.52	1.39	0.36	5.81
A ₀₂ ^r	190	61.4	5.82	113	1.97	1.53	28.0
A ₂₀ ^r	189	11.3	6.73	4.07	13.2	5.79	8.58
A ₁₁ ^r	188	6.55	0.97	0.66	13.7	4.94	5.32
A ₁₂ ^r	189	>500	>500	>500	>500	>500	>500
A ₂₁ ^r	183	14.6	26.4	5.87	29.2	12.5	20.6
A ₃₀ ^r	191	32.6	45.4	14.4	34.0	19.9	33.6
Johnson <i>et al.</i> ³							
A ₀₀ ^r	191	0.69	0.68	2.26	11.9	2.73	2.66
A ₀₁ ^r	191	0.38	3.85	3.83	2.58	0.83	2.43
A ₁₀ ^r	191	18.4	0.13	0.45	1.32	0.32	5.54
A ₀₂ ^r	190	61.7	5.83	115	2.94	1.22	28.5
A ₂₀ ^r	189	12.4	7.90	4.12	13.2	5.68	9.16
A ₁₁ ^r	188	7.50	1.32	0.62	14.2	5.02	5.73
A ₁₂ ^r	189	>500	>500	>500	>500	>500	>500
A ₂₁ ^r	189	15.6	33.6	6.15	38.5	13.7	25.5
A ₃₀ ^r	183	34.4	53.1	15.7	34.1	18.8	36.5

^aSupercritical fluid: LD: $\rho/\rho_c < 0.6$; MD: $0.6 \leq \rho/\rho_c \leq 1.5$; HD: $\rho/\rho_c > 1.5$.

During the fitting procedure, some general aspects of the simulation data must be considered. Temperature derivatives of the Helmholtz energy are usually less uncertain than density derivatives. The equation of state then represents temperature derivatives such as heat capacities better than density derivatives such as compressibilities. The accuracy of all derivatives decreases with increasing order of the derivative. The residual Helmholtz energy itself has to be treated differently because of a possible breakdown of the test-particle method at high density. Furthermore, molecular simulation yields higher relative uncertainties in the gaseous phase than in the liquid phase. Finally, zero crossings occur for some derivatives (e.g., A_{01}^r), which may obscure deviation plots. Here, only selected isotherms are presented for each derivative. A comprehensive overview is given in the supplementary material.⁵² For each isotherm, the EOS of Mecke *et al.*⁵ is used for comparison. Additionally, average absolute relative deviations (AAD) are presented in Table 5.

Deviations of residual Helmholtz energy A_{00}^r data are illustrated in Fig. 5. A_{00}^r is generally reproduced within 0.5% (AAD = 0.46%). However, there are differences depending on temperature and density range. For example, A_{00}^r in the gaseous phase ($T = 0.8$ – 1.2) is reproduced within less than 0.2%, whereas the deviations of the low-density data

in the supercritical state increase up to 0.5% (e.g., $T = 7$). Some isotherms show scatter of the data (e.g., $T = 1.5$ – 3), whereas higher temperatures are entirely consistent ($T = 7$ – 9).

In comparison, modeling the first density derivative A_{01}^r is more challenging than A_{00}^r , as shown in Fig. 6. Although the deviation plots show oscillations (e.g., $T = 4$ – 9), the accuracy of the equation of state is still within 0.5%. Both the equations of Mecke *et al.*⁵ and of this work show similar behavior. The AAD of the present EOS improves over the entire surface: 0.49% vs. 1.01% for Mecke *et al.*⁵ The isotherm $T = 4$ illustrates the difference between low- and high-density simulations. The uncertainty of the data decreases with increasing density. The isotherm $T = 3$ shows scatter in the data for $\rho < 0.45$. Such regions have to be treated carefully to avoid overfitting so that the equation is not forced to follow the scatter of the data.

The first temperature derivative A_{10}^r shown in Fig. 7 is the most accurate property to determine from molecular simulation. The liquid phase is represented within 0.03% (AAD = 0.02%). The low-density data are more challenging. In the gas phase, they are reproduced within 0.5% (AAD = 0.28%). Since the vapor–liquid equilibrium is located between the gaseous and liquid data, it is difficult to assess

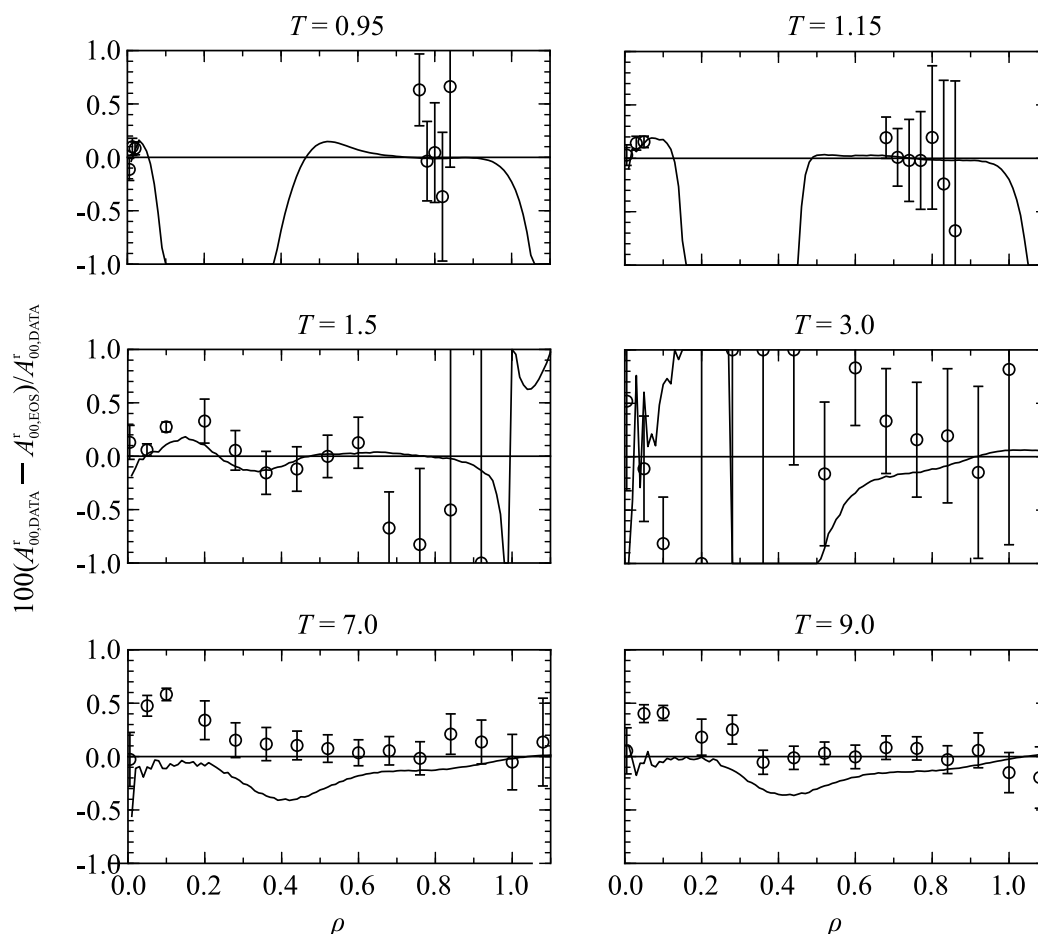


FIG. 5. Relative deviation of simulated residual Helmholtz energy A_{00}^r data (circles) from the present equation of state. The equation of Mecke *et al.*⁵ (solid curve) is plotted for comparison.

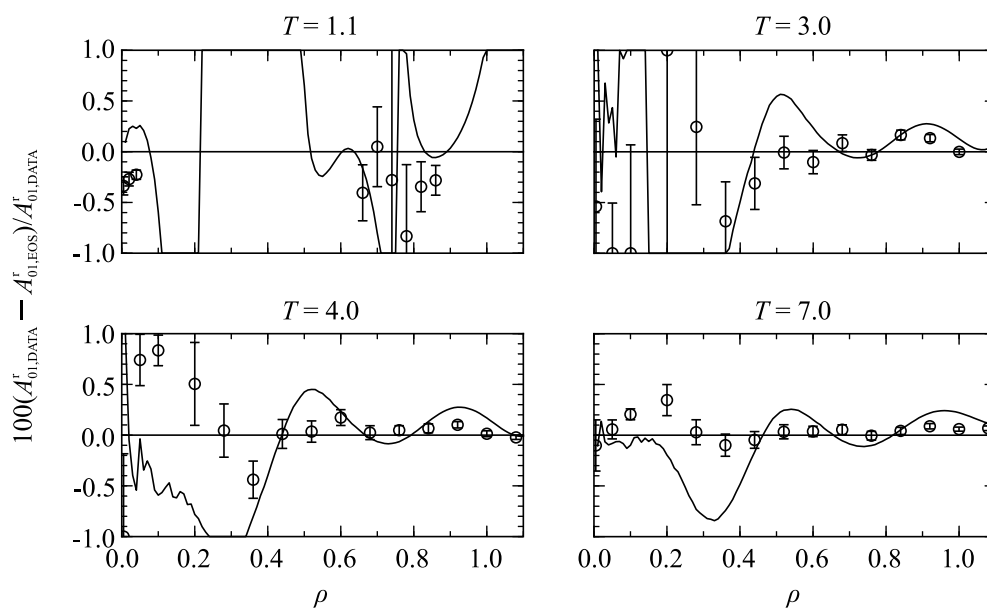


FIG. 6. Relative deviation of simulated first derivative of the residual Helmholtz energy with respect to density A'_{01} data (circles) from the present equation of state. The equation of Mecke *et al.*⁵ (solid curve) is plotted for comparison.

a correct transition between low- and high-density data. The supercritical state allows for a continuous evaluation of the data over the entire density range. At $T = 3$ and 5, a consistent trend persists over the entire density range. In contrast, T

$= 1.5$ and 2 show an offset of the relative deviations between low-density and medium-density data. Isotherms $T = 7$ and 9 were fitted less accurately. During the fit, it was not possible to improve accuracy without compromising lower isotherms.

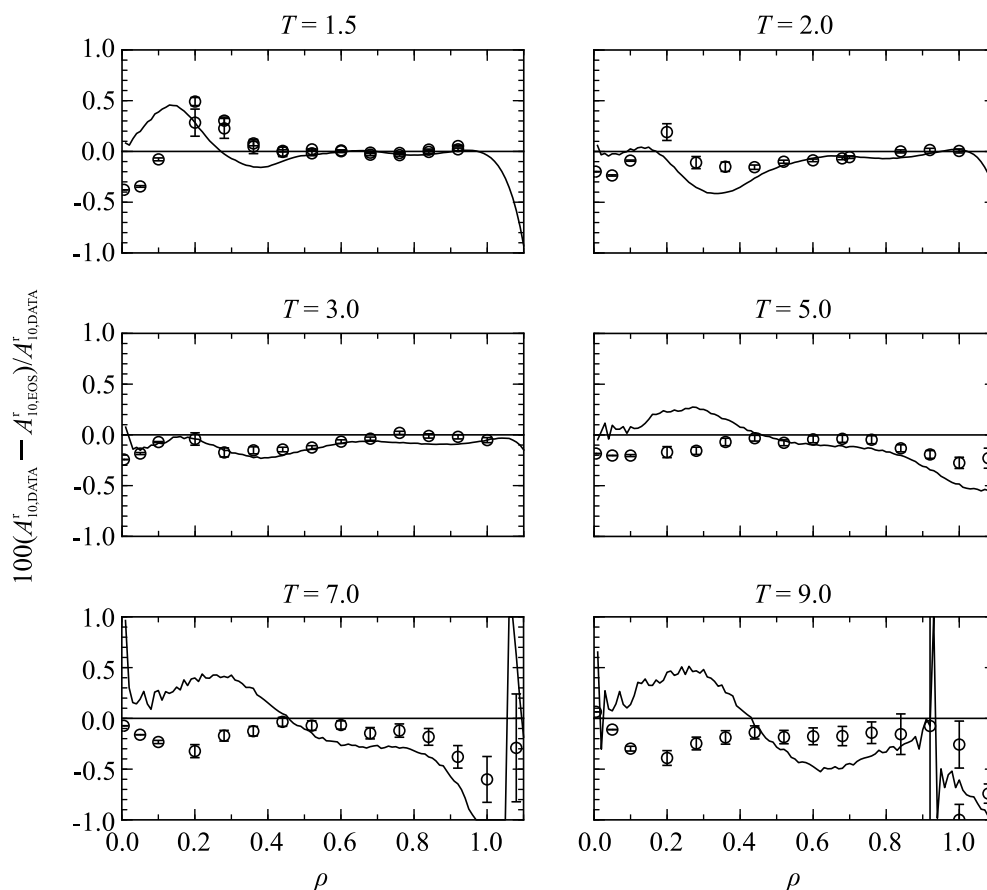


FIG. 7. Relative deviation of simulated first derivative of the residual Helmholtz energy with respect to inverse temperature A'_{10} data (circles) from the present equation of state. The equation of Mecke *et al.*⁵ (solid curve) is plotted for comparison.

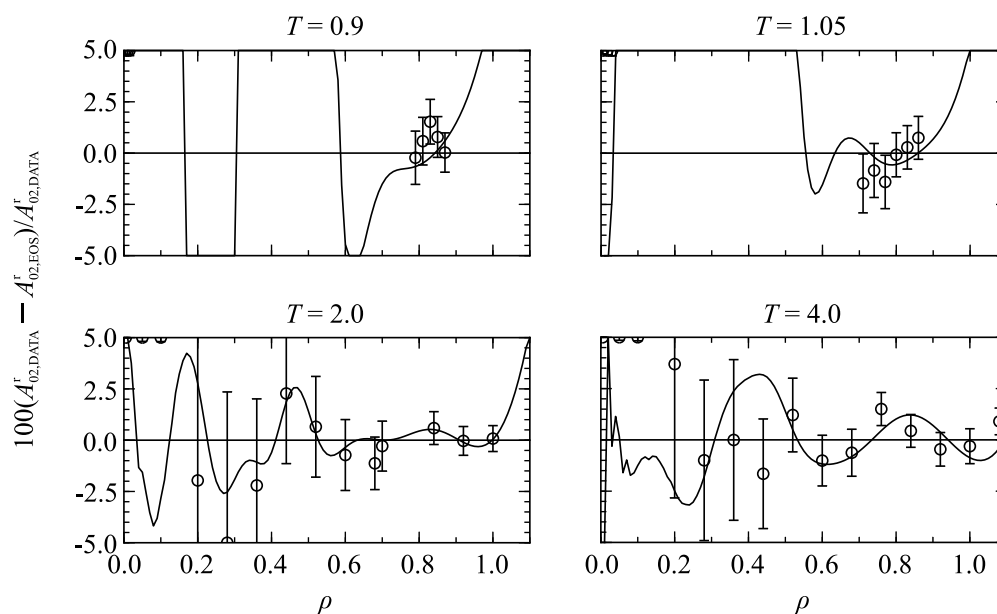


FIG. 8. Relative deviation of simulated second derivative of the residual Helmholtz energy with respect to density A_{02}^r data (circles) from the present equation of state. The equation of Mecke *et al.*⁵ (solid curve) is plotted for comparison.

Therefore, uncertainties in the supercritical state are 0.2% for $T < 7$ and up to 0.6% for $T \geq 7$. The overall AAD of this work and Mecke *et al.*⁵ are quite similar: 0.14% vs. 0.16%, respectively.

The second density derivative A_{02}^r in Fig. 8 is similarly represented with AAD = 28.0% versus 27.8% for Mecke *et al.*⁵ High AAD in the low-density region are caused by small numerical values resulting in a high relative deviation. In the liquid region, the data are represented within 1.5%. Both equations show about the same deviations. Similar to A_{01}^r , deviations in the supercritical region oscillate. Scatter occurs at medium temperatures ($T = 1.5$ – 5) and $\rho < 0.45$. The error of calculated A_{02}^r data in the supercritical region was estimated

to be 2.5% for $\rho < 0.45$ (AAD_{MD} = 2.66%) and 1.5% for $\rho \geq 0.45$ (AAD_{HD} = 0.85%).

Figure 9 shows that A_{20}^r behaves as smooth as A_{10}^r . A significant oscillation can be observed for medium temperatures. The gaseous and liquid regions are described with an accuracy of better than 1% (AAD_{gas} = 0.47% and AAD_{liq} = 0.40%), which is a large improvement in comparison with the EOS of Mecke *et al.*⁵ (AAD_{gas} = 1.07% and AAD_{liq} = 0.88%). For $T \geq 3$, medium- and high-density data are reproduced within 0.5%. The transition of the low-density into the medium-density range shows an offset. Therefore, the uncertainty is 1%, although the data have lower statistical uncertainties. The supercritical region represents a significant improvement over

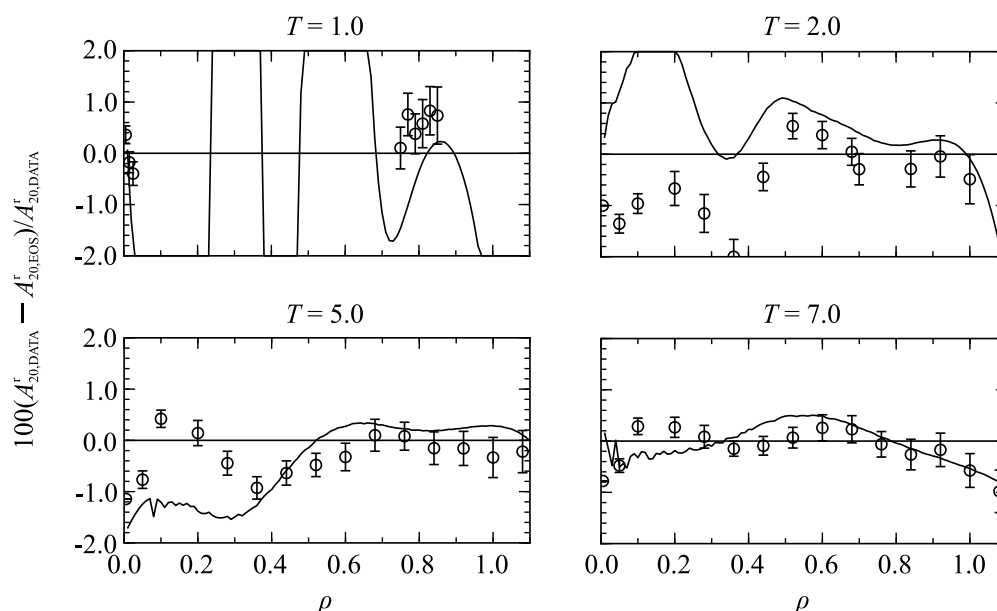


FIG. 9. Relative deviation of simulated second derivative of the residual Helmholtz energy with respect to inverse temperature A_{20}^r data (circles) from the present equation of state. The equation of Mecke *et al.*⁵ (solid curve) is plotted for comparison.

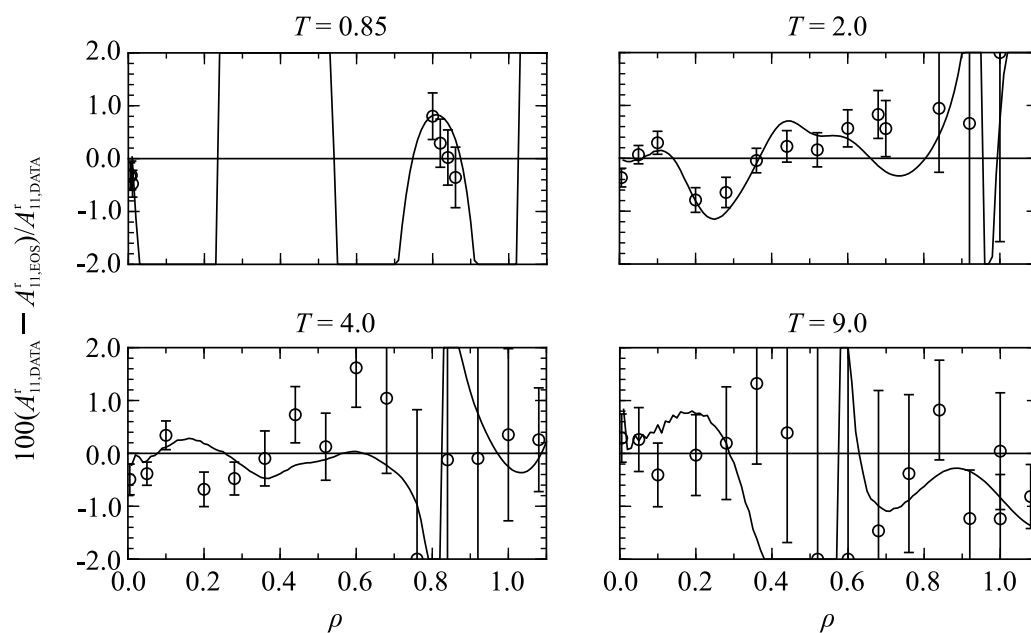


FIG. 10. Relative deviation of simulated mixed derivative of the residual Helmholtz energy with respect to density and inverse temperature A_{11}^r data (circles) from the present equation of state. The equation of Mecke *et al.*⁵ (solid curve) is plotted for comparison.

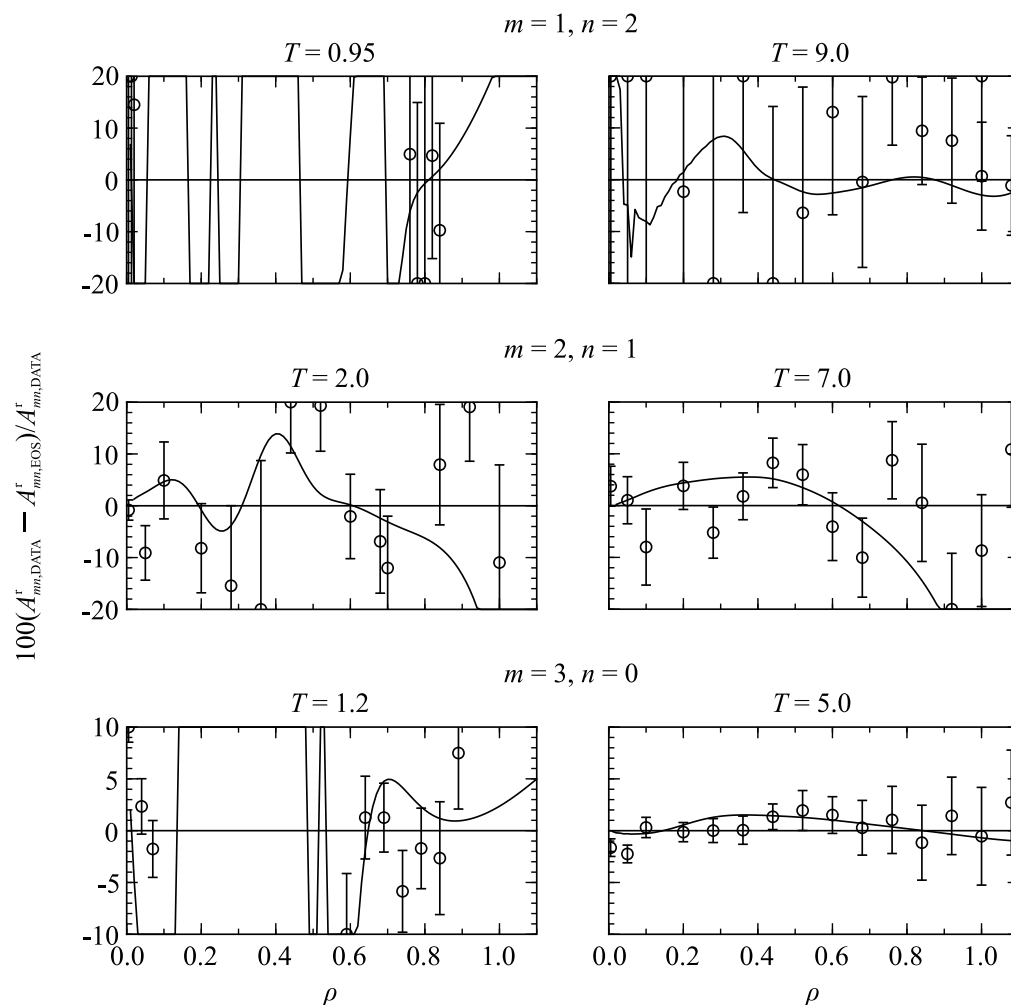


FIG. 11. Relative deviation of the simulated third derivatives of the residual Helmholtz energy with respect to density and inverse temperature data (circles) from the present equation of state: first row A_{12}^r , second row A_{21}^r , third row A_{30}^r . The equation of Mecke *et al.*⁵ (solid curve) is plotted for comparison.

Mecke *et al.*⁵ The overall AAD is decreased from the previous 0.93% to 0.48% in this work.

Figure 10 shows the mixed derivative A_{11}^T . The gaseous region is represented within 0.5% (AAD = 0.33%), whereas the deviation in the liquid region increases from 0.5% to 1% toward high densities (AAD = 0.49%). In the supercritical region at densities $\rho \leq 0.5$, the accuracy is within 1% (AAD_{LD} = 0.28% and AAD_{MD} = 0.34%). For $\rho > 0.5$, significant scatter occurs with an estimated uncertainty of more than 3%. The overall AAD of both equations is quite similar and no noticeable improvement is achieved.

Third-order derivatives are currently associated with too large statistical uncertainties to be used to parameterize the equation of state and were used for comparison only. At least the third inverse temperature derivative A_{30}^T shows acceptable deviations with an overall AAD = 4.44% (cf. Fig. 11). Especially in the supercritical region for $T \geq 4$, the equation shows agreement with the simulation data within about 3%. Other regions are reproduced within 5%–10%. The deviations of calculated A_{12}^T data are at least 20% (overall AAD = 88.2%

caused by low-density data). A_{21}^T data are reproduced within 20% for $T \leq 2$ and 10% for $T > 2$ (overall AAD = 12.8%). The deviations with respect to the EOS of Mecke *et al.*⁵ are slightly higher for these properties.

5.2. Thermal virial coefficients

In addition to the residual Helmholtz derivatives, which are exclusively located in the homogeneous region, the gas phase was modeled with virial coefficients up to the fourth. Second (B) and third (C) virial coefficients were used to set up previous equations of state (cf. Table 4). Available data from the literature, e.g., Nicolas *et al.*,²⁵ Barker *et al.*,²⁹ Shaul *et al.*,⁵³ Bird *et al.*,⁵⁴ Hirschfelder *et al.*,⁵⁵ Sun and Teja,⁵⁶ and others, are augmented by “exact” calculations provided by Wheatley.³³ Figure 12 displays details. For clarity, only virial coefficient data of Sun and Teja⁵⁶ and Wheatley³³ are plotted.

The second virial coefficient from the present EOS represents all available data. The EOS of Mecke *et al.*⁵ follows

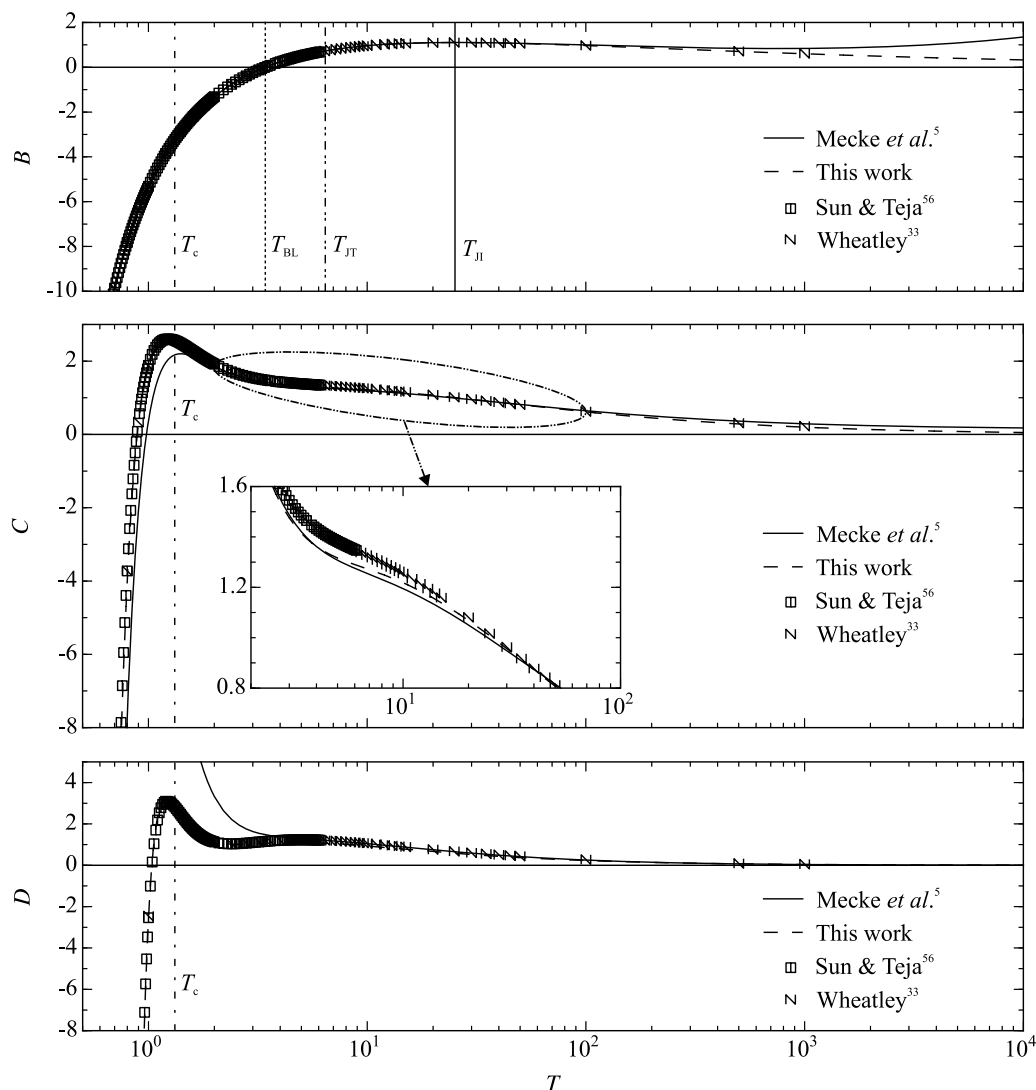


FIG. 12. Second, third, and fourth thermal virial coefficients. The critical temperature T_c , Boyle temperature T_{BL} , Joule–Thomson inversion temperature T_{JT} , and Joule inversion temperature T_{JI} are indicated.

TABLE 6. Selected points on the characteristic ideal curves calculated with the present equation of state

Property	T	ρ	p
Temperature of Boyle curve in the zero-density limit	3.417		
Joule–Thomson inversion temperature in the zero-density limit	6.425		
Joule inversion temperature in the zero-density limit	25.17		
Maximum of Joule–Thomson inversion curve	2.917	0.387	1.386
Intersection of Joule–Thomson inversion curve and saturated liquid line	1.051	0.673	0.035

the exact second virial coefficient up to $T = 100$, which was reported to be the upper range for a reasonable extrapolation behavior.⁵ For higher temperatures, the two equations differ from each other. The present EOS follows the calculated second virial coefficient of Wheatley³³ approaching zero, whereas that of Mecke *et al.*⁵ does not. The Boyle temperature, Joule–Thomson inversion temperature, and Joule inversion temperature in the zero-density limit are also indicated in Fig. 12. They are in good agreement with values of Hirschfelder *et al.*⁵⁵ ($T_{BL} = 3.42$), Friedrich and Lustig⁵⁷ ($T_{BL} = 3.41$, $T_{JT} = 6.47$), Breitenstein and Lustig⁵⁸ ($T_{BL} = 3.42$, $T_{JT} = 6.43$), and Breitenstein⁵⁹ ($T_{BL} = 3.4179$, $T_{JT} = 6.4308$). The exact Joule inversion temperature has not yet been established in the literature. Additional characteristic properties calculated from the present EOS can be found in Table 6.

In addition to the second virial coefficient, its first temperature derivative (dB/dT) was reported by Hirschfelder *et al.*⁵⁵ As expected, both equations agree with these data for $T \leq 100$. For higher temperatures, an unphysical slope for B of the equation of Mecke *et al.*⁵ (cf. Fig. 12) is also visible in Fig. 13 because the temperature derivative is positive. In compar-

ison, the present EOS exhibits a correct negative temperature derivative in that range. However, it is important to keep in mind that the temperature $T/T_c \approx 75$ is well beyond the range of validity of both equations.

The third virial coefficient is reproduced by the present EOS as accurately as the second virial coefficient, except for the region near the maximum. As the Lennard-Jones fluid is a simple monatomic model, a similar behavior as the equation for argon by Tegeler *et al.*⁶⁰ is expected. Their EOS as well as third virial coefficient data determined from highly accurate $p\rho T$ measurements by Gilgen *et al.*⁶¹ show a maximum slightly below the critical temperature. Figure 12 shows that this is also true for the Lennard-Jones fluid. This behavior is in agreement with the available data. An inflection point in C is obvious from Fig. 12. Additionally, exact calculations for the first temperature derivative of the third virial coefficient were provided by both Hirschfelder *et al.*⁵⁵ and Bird *et al.*⁵⁴ In Fig. 13, the inflection point is clearly illustrated by a maximum in the temperature derivative around $T = 6$.

On the bottom panel of Fig. 12, the fourth virial coefficient is shown. The available data from exact calculations^{33,56} as

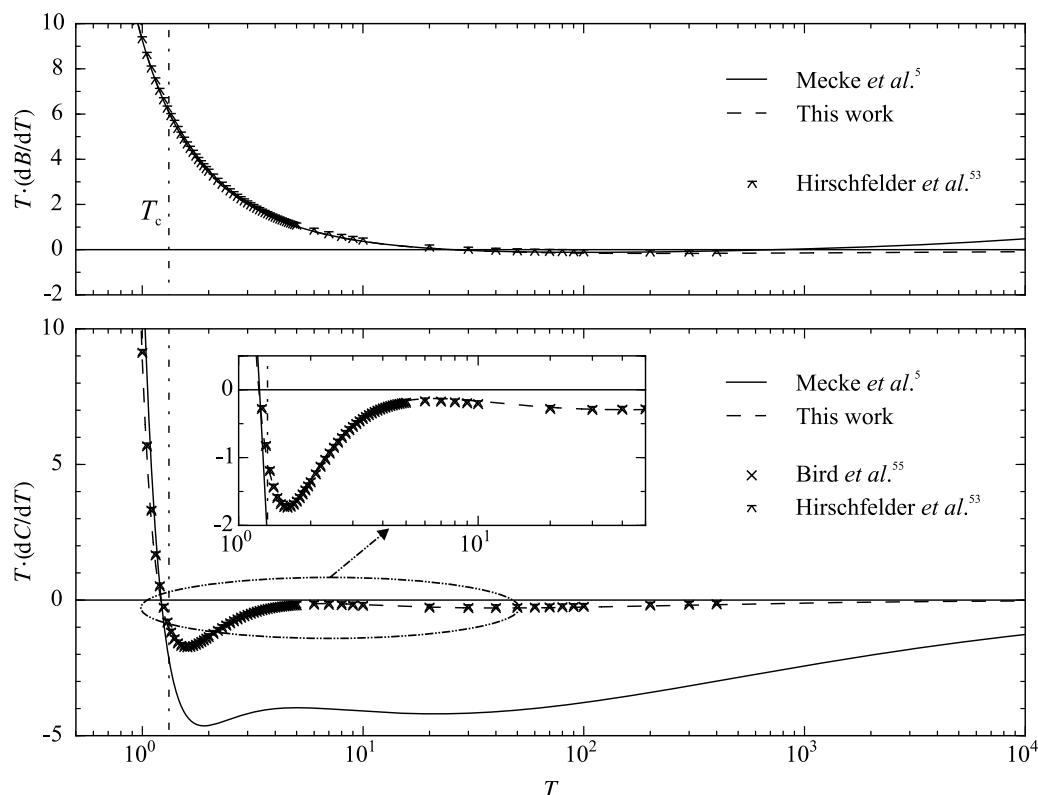


Fig. 13. First derivative of the second and third thermal virial coefficients with respect to temperature.

well as the present equation of state show a first maximum around the critical temperature and a second less pronounced maximum at $T \approx 4.8$. As discussed by Thol *et al.*,⁶² the fourth virial coefficient has rarely been investigated in the context of equations of state and few experimental measurements are available for real fluids. However, no measurements of D exist in the temperature region where the second maximum occurs ($T/T_c \approx 3.6$).

5.3. Vapor–liquid equilibrium

The present equation of state is exclusively based on Helmholtz energy derivatives at homogeneous states and on thermal virial coefficients. Therefore, vapor–liquid equilibrium is output of, and not input to, the fitting procedure. Figure 14 shows relative deviations of available data for vapor pressure p_v , saturated liquid density ρ' , and saturated vapor density ρ'' .

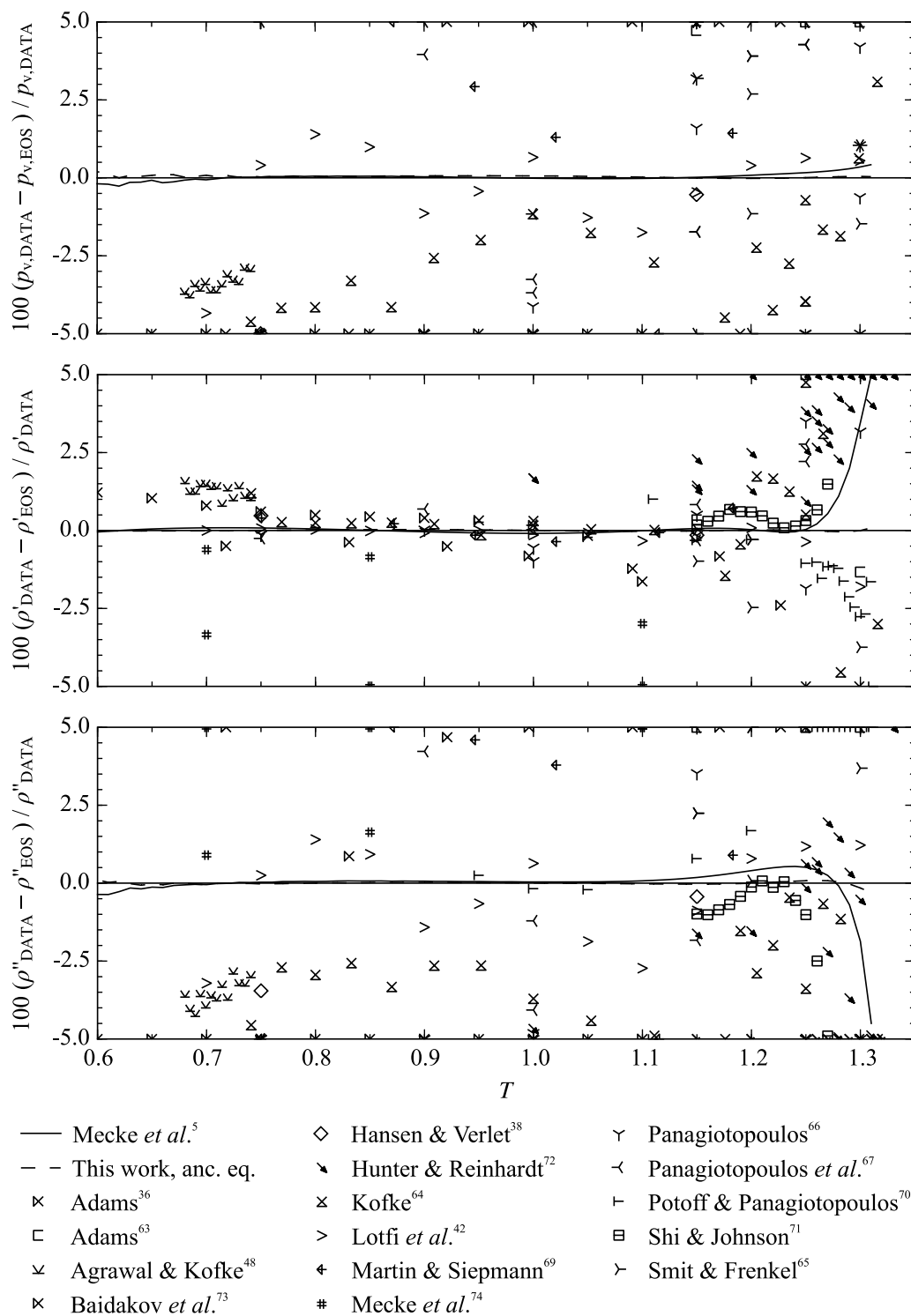


Fig. 14. Relative deviation of literature data for vapor pressure, saturated liquid density, and saturated vapor density from the present equation of state.

TABLE 7. Parameters of the ancillary equations for vapor pressure, saturated liquid density, and saturated vapor density

<i>i</i>	Vapor pressure, Eq. (44)		Saturated liquid density, Eq. (45)		Saturated vapor density, Eq. (46)	
	n_i	t_i	n_i	t_i	n_i	t_i
1	$-0.540\,00 \times 10^{+1}$	1.00	$0.1362 \times 10^{+1}$	0.313	$-0.696\,55 \times 10^{+1}$	1.320
2	$0.447\,04 \times 10^0$	1.50	$0.2093 \times 10^{+1}$	0.940	$-0.103\,31 \times 10^{+3}$	19.24
3	$-0.185\,30 \times 10^{+1}$	4.70	$-0.2110 \times 10^{+1}$	1.630	$-0.203\,25 \times 10^{+1}$	0.360
4	$0.198\,90 \times 10^0$	2.50	0.3290×10^0	17.00	$-0.444\,81 \times 10^{+2}$	8.780
5	$-0.112\,50 \times 10^{+1}$	21.4	$0.1410 \times 10^{+1}$	2.400	$-0.184\,63 \times 10^{+2}$	4.040
6					$-0.260\,70 \times 10^{+3}$	41.60

TABLE 8. Average absolute relative deviations of vapor pressure, saturated liquid density, and saturated vapor density from literature data relative to the present equation of state

Authors	No. of data	Temperature range	Average absolute relative deviations/%			
			LT ^a	MT ^a	HT ^a	overall
Vapor pressure p_v						
Adams ³⁶	11	0.60–1.10	10.2	9.49	–	9.76
Adams ⁶³	3	1.15–1.30	–	8.81	5.72	7.78
Agrawal and Kofke ⁴⁸	13	0.68–0.74	3.35	–	–	3.35
Baidakov <i>et al.</i> ^{73 b}	7	0.72–1.23	25.0	22.0	–	22.4
Hansen and Verlet ³⁸	2	0.75–1.15	5.17	0.54	–	2.86
Kofke ⁶⁴	22	0.74–1.32	4.39	2.99	1.86	3.01
Lotfi <i>et al.</i> ⁴²	13	0.70–1.30	2.37	0.91	0.55	1.11
Martin and Siepmann ⁶⁹	6	0.75–1.18	17.0	3.85	–	6.03
Panagiotopoulos ⁶⁶	22	0.75–1.30	45.5	97.2	2.73	70.6
Panagiotopoulos <i>et al.</i> ⁶⁷	18	0.75–1.30	50.2	6.84	3.01	11.2
Smit and Frenkel ⁶⁵	12	1.15–1.30	–	9.05	1.26	7.75
Saturated liquid density ρ'						
Adams ³⁶	11	0.60–1.10	0.92	0.52	–	0.67
Adams ⁶³	3	1.15–1.30	–	2.90	1.33	2.38
Agrawal and Kofke ⁴⁸	13	0.68–0.74	1.31	–	–	1.31
Baidakov <i>et al.</i> ^{73 b}	7	0.72–1.23	0.50	1.02	–	0.95
Hansen and Verlet ³⁸	2	0.75–1.15	0.48	0.15	–	0.31
Kofke ⁶⁴	22	0.74–1.32	0.74	1.69	4.92	1.90
Lotfi <i>et al.</i> ⁴²	13	0.70–1.30	0.03	0.14	1.81	0.25
Martin and Siepmann ⁶⁹	6	0.75–1.18	0.40	0.30	–	0.32
Mecke <i>et al.</i> ⁷⁴	6	0.70–1.10	1.98	6.17	–	4.77
Panagiotopoulos ⁶⁶	11	0.75–1.30	0.13	1.08	5.23	1.66
Panagiotopoulos <i>et al.</i> ⁶⁷	9	0.75–1.30	0.25	1.00	5.28	1.39
Potoff and Panagiotopoulos ⁷⁰	19	0.95–1.31	–	0.93	7.24	2.59
Shi and Johnson ⁷¹	13	1.15–1.27	–	0.48	–	0.48
Smit and Frenkel ⁶⁵	6	1.15–1.30	–	0.81	3.74	1.30
Saturated vapor density ρ''						
Adams ³⁶	11	0.60–1.10	10.4	12.0	–	11.4
Adams ⁶³	3	1.15–1.30	–	17.9	12.4	16.1
Agrawal and Kofke ⁴⁸	13	0.68–0.74	3.49	–	–	3.49
Baidakov <i>et al.</i> ^{73 b}	7	0.72–1.23	13.9	6.95	–	7.95
Hansen and Verlet ³⁸	2	0.75–1.15	3.46	0.44	–	1.95
Kofke ⁶⁴	22	0.74–1.32	3.62	5.87	17.5	6.72
Lotfi <i>et al.</i> ⁴²	13	0.70–1.30	1.73	1.25	1.22	1.32
Martin and Siepmann ⁶⁹	6	0.75–1.18	16.8	5.80	–	7.64
Mecke <i>et al.</i> ⁷⁴	6	0.70–1.10	29.9	22.7	–	25.1
Panagiotopoulos ⁶⁶	11	0.75–1.30	31.7	11.6	16.5	16.2
Panagiotopoulos <i>et al.</i> ⁶⁷	9	0.75–1.30	16.8	6.65	8.28	7.96
Potoff and Panagiotopoulos ⁷⁰	19	0.95–1.31	–	4.17	13.2	6.54
Shi and Johnson ⁷¹	13	1.15–1.27	–	1.02	–	1.02
Smit and Frenkel ⁶⁵	6	1.15–1.30	–	7.76	3.69	7.08

^aLT: $T/T_c < 0.6$; MT: $0.6 \leq T/T_c \leq 0.98$; HT: $T/T_c > 0.98$.^bTruncated at 6.78σ .

TABLE 9. Average absolute relative deviations of simulation data in homogeneous states from the literature relative to the present equation of state. For the $p\rho T$ data in the critical region, pressure deviations are considered instead of density deviations. Critical region: $0.98 \leq T/T_c \leq 1.1$ and $0.7 \leq \rho/\rho_c \leq 1.4$; Supercritical region: LD: $\rho/\rho_c < 0.6$; MD: $0.6 \leq \rho/\rho_c \leq 1.5$; HD: $\rho/\rho_c > 1.5$

Authors	No. of data	Temperature and pressure range		Average absolute relative deviations (AAD)/%						Overall
							Supercritical fluid			
		T	p	Gas	Liq.	Crit. Reg.	LD	MD	HD	
$p\rho T$ data										
Adams ³⁵	12	2.00–4.00	0.08–15.06	–	–	–	2.77	2.39	0.71	1.99
Adams ³⁶	16	1.00–1.20	0.06–1.37	–	0.81	–	–	–	–	0.81
Adams ⁶³	28	1.15–1.35	0.04–0.35	3.31	0.72	3.03	2.84	7.11	–	2.40
Baidakov <i>et al.</i> ⁷³	99	0.70–2.00	0.00–15.19	1.43	0.06	0.88	0.08	0.65	0.04	0.43
Carley ⁷⁶	11	1.35	0.15–0.75	–	–	1.34	–	5.02	0.75	1.74
Fickett and Wood ⁷⁷	23	1.96–181.14	12.20–1463.83	–	–	–	–	–	2.89	2.89
Hansen ³⁷	7	2.74–100.00	1.32–666.4	–	–	–	–	0.23	0.34	0.32
Hansen and Verlet ³⁸	7	0.75–1.15	0.00–5.00	0.13	1.07	–	–	–	–	0.80
Johnson <i>et al.</i> ³	151	0.80–6.00	0.00–85.71	0.17	0.05	0.94	0.14	0.28	0.08	0.14
Kolafa and Nezbeda ⁴	11	0.81–10.00	0.11–99.18	–	0.19	2.12	–	0.45	0.05	0.70
Kolafa <i>et al.</i> ³⁹	45	0.72–4.85	0.03–31.32	0.19	1.88	2.02	–	0.09	0.16	1.25
Levesque and Verlet ²²	17	1.35	0.14–8.11	–	–	36.8	322	192	13.3	48.9
Lotfi <i>et al.</i> ⁴²	4	0.95–1.30	0.00–0.12	–	0.18	1.57	–	–	–	0.53
Lustig ⁷	2	1.18	0.58–0.59	–	0.29	–	–	–	–	0.29
Lustig ¹⁷	8	1.01–3.00	0.20–8.22	–	0.21	0.68	–	0.03	0.07	0.25
May and Mausbach ¹⁶	193	0.70–6.17	0.09–99.97	2.48	0.35	2.59	0.63	1.12	0.12	0.53
McDonald and Singer ⁷⁸	21	0.72–1.24	0.00–1.56	–	0.68	–	–	–	–	0.68
McDonald and Singer ²³	44	0.72–1.24	0.00–1.64	–	0.43	–	–	–	–	0.43
McDonald and Singer ⁷⁹	19	0.72–1.24	0.00–1.34	–	0.68	–	–	–	–	0.68
McDonald and Singer ⁸⁰	48	1.45–3.53	0.15–6.26	–	–	6.74	0.88	1.08	0.88	1.04
McDonald and Woodcock ⁸¹	3	1.05–2.33	0.01–3.52	–	0.91	–	–	0.40	0.23	0.51
Mecke <i>et al.</i> ⁵	12	1.32–1.33	0.13–0.16	–	–	1.19	–	0.99	–	1.12
Meier ¹⁴	297	0.70–6.00	0.00–92.95	0.33	0.07	0.63	0.11	0.21	0.05	0.14
Miyano ²⁷	71	1.31–100.00	0.00–297.00	–	–	3.83	–	0.59	0.15	1.95
Morsali <i>et al.</i> ⁸²	13	5.01	2.58–41.55	–	–	–	–	0.04	0.08	0.08
Nicolas <i>et al.</i> ²⁵	55	1.03–6.01	0.20–72.84	–	0.56	8.24	–	1.13	0.23	0.54
Ree ⁸³	12	0.81–2.70	0.44–4.37	–	0.46	–	1.20	0.25	0.56	0.51
Saager and Fischer ⁴⁰	26	0.68–4.00	0.00–27.07	–	0.11	–	–	0.28	0.08	0.12
Schofield ⁸⁴	2	0.73	0.14–0.95	–	2.63	–	–	–	–	2.63
Shaw ⁸⁵	240	0.70–136.25	0.12–555.66	–	0.48	–	–	–	0.46	0.47
Sowers and Sandler ⁸⁶	60	1.35–6.00	0.06–25.88	–	–	4.27	0.34	0.43	0.32	0.48
Streett <i>et al.</i> ⁸⁷	76	1.00–3.05	0.00–32.61	–	2.58	–	–	–	1.95	2.37
Toxvaerd and Praestgaard ⁸⁸	8	1.35	0.14–5.56	–	–	5.41	–	–	0.72	2.48
Verlet and Levesque ⁸⁹	5	1.35–2.74	0.15–2.43	–	–	1.98	–	7.54	1.42	2.87
Verlet ⁴¹	32	0.72–4.62	0.20–10.71	–	0.17	1.53	–	2.96	6.67	2.98
Weeks <i>et al.</i> ⁹⁰	5	0.75–1.35	0.23–5.56	–	0.18	–	–	–	0.33	0.24
Wood ⁹¹	28	1.06–100.00	0.00–584.94	–	5.63	–	–	–	0.57	1.65
Wood and Parker ⁹²	12	2.74	0.00–7.36	–	–	–	–	5.17	16.5	12.7
Residual internal energy u^r										
Adams ³⁵	12	2.00–4.00	0.08–14.99	–	–	–	2.48	1.48	0.92	1.71
Adams ³⁶	16	1.00–1.20	0.09–1.34	–	0.67	–	–	–	–	0.67
Adams ⁶³	28	1.15–1.35	0.04–0.34	0.37	0.15	1.31	0.39	0.28	–	0.44
Baidakov <i>et al.</i> ⁷³	99	0.70–2.00	0.00–15.21	0.70	0.06	0.74	0.24	0.27	0.05	0.27
Hansen ³⁷	7	2.74–100.00	1.32–645.59	–	–	–	–	0.10	0.83	0.73
Johnson <i>et al.</i> ³	151	0.80–6.00	0.00–84.90	2.28	0.03	0.32	0.34	0.21	0.29	0.37
Kolafa <i>et al.</i> ³⁹	45	0.72–4.85	0.04–31.47	0.58	0.06	2.96	–	0.18	0.19	0.72
Kolafa and Nezbeda ⁴	11	0.81–10.00	0.12–98.73	–	0.08	0.50	–	0.89	0.97	0.51
Levesque and Verlet ²²	32	0.72–3.67	0.15–28.19	–	0.30	2.54	–	0.36	1.04	1.04
Lotfi <i>et al.</i> ⁴²	5	0.75–1.30	0.00–0.12	–	0.07	0.07	–	–	–	0.07
May and Mausbach ¹⁶	193	0.70–6.17	0.00–98.13	0.48	0.02	0.28	0.13	0.14	0.26	0.20
McDonald and Singer ⁷⁸	23	0.72–1.24	0.00–1.69	–	15.6	–	–	–	–	15.6
McDonald and Singer ²³	45	0.72–1.24	0.00–1.69	–	0.38	–	–	–	–	0.38
McDonald and Singer ⁷⁹	20	0.72–1.24	0.00–1.10	–	0.69	–	–	–	–	0.69
McDonald and Singer ⁸⁰	48	1.45–3.53	0.15–6.36	–	–	3.85	3.49	1.95	0.74	1.77
McDonald and Woodcock ⁸¹	5	0.75–2.33	0.04–3.54	–	0.37	–	–	0.28	0.13	0.30
Mecke <i>et al.</i> ⁵	12	1.32–1.33	0.13–0.16	–	–	0.62	–	0.63	–	0.62
Meier ¹⁴	299	0.70–6.00	0.00–91.66	0.30	0.02	0.53	0.15	0.15	0.27	0.21
Miyano ²⁷	71	1.31–100.00	0.00–293.24	–	–	1.80	–	8.42	3.47	3.74
Nicolas <i>et al.</i> ²⁵	55	1.03–6.01	0.22–72.61	–	0.17	1.95	–	0.95	0.78	0.78
Ree ⁸³	12	0.81–2.70	0.45–4.45	–	0.28	–	3.25	1.86	0.73	0.70

TABLE 9. Average absolute relative deviations of simulation data in homogeneous states from the literature relative to the present equation of state. For the $p\rho T$ data in the critical region, pressure deviations are considered instead of density deviations. Critical region: $0.98 \leq T/T_c \leq 1.1$ and $0.7 \leq \rho/\rho_c \leq 1.4$; Supercritical region: LD: $\rho/\rho_c < 0.6$; MD: $0.6 \leq \rho/\rho_c \leq 1.5$; HD: $\rho/\rho_c > 1.5$ —Continued

Authors	No. of data	Temperature and pressure range		Average absolute relative deviations (AAD)/%						
							Supercritical fluid			Overall
		T	p	Gas	Liq.	Crit. Reg.	LD	MD	HD	
Saager and Fischer ⁴⁰	26	0.68–4.00	0.00–27.04	–	0.06	–	–	0.41	0.23	0.21
Shaw ⁸⁵	243	0.66–136.25	0.02–549.83	–	0.20	–	–	–	1.62	1.20
Sowers and Sandler ⁸⁶	54	1.35–6.00	0.10–25.93	–	–	1.94	0.64	0.73	0.54	0.66
Streett <i>et al.</i> ⁸⁷	76	1.00–3.05	0.00–33.80	–	2.87	–	–	–	9.46	5.13
Verlet ⁴¹	32	0.72–4.62	0.20–10.69	–	0.68	5.14	–	0.71	0.19	0.81
Verlet and Levesque ⁸⁹	6	1.35–2.74	0.15–2.56	–	–	0.80	–	1.96	1.64	1.41
Wood ⁹¹	48	1.06–100.00	0.00–3236.83	–	2.92	–	–	–	5.89	5.52
Wood and Parker ⁹²	12	2.74	0.00–20.82	–	–	–	–	45.0	31.4	36.0
Isochoric heat capacity c_v										
Adams ³⁵	12	2.00–4.00	0.08–14.99	–	–	–	0.22	1.17	0.66	0.60
Adams ⁶³	27	1.15–1.35	0.04–0.34	1.43	4.35	2.33	0.72	3.09	–	2.96
Baidakov <i>et al.</i> ⁷³	97	0.70–2.00	0.00–15.21	1.55	0.42	2.93	0.96	0.96	0.23	0.84
Boda <i>et al.</i> ⁹³	8	1.35–2.00	0.15–0.51	–	–	4.72	–	0.47	–	1.53
May and Mausbach ¹⁶	192	0.70–6.17	0.00–98.13	1.74	0.35	6.89	0.18	0.35	0.13	0.41
McDonald and Singer ⁷⁹	20	0.72–1.24	0.00–1.10	–	7.99	–	–	–	–	7.99
McDonald and Singer ⁸⁰	48	1.45–3.53	0.15–6.36	–	–	9.48	2.39	1.85	1.33	1.88
Meier ¹⁴	282	0.70–6.00	0.00–91.66	0.40	0.34	5.10	0.15	0.42	0.20	0.48
Szalai <i>et al.</i> ⁹⁴	4	1.10–1.35	0.05–0.14	1.90	–	–	–	1.65	–	1.84
Wood and Parker ⁹²	12	2.74	0.00–20.82	–	–	–	–	2.98	25.7	18.5
Isobaric heat capacity c_p										
Boda <i>et al.</i> ⁹³	39	0.75–1.90	0.00–0.25	0.95	2.98	1.07	1.88	2.41	2.76	2.33
Lustig ¹⁷	6	1.01–3.00	0.61–8.22	–	–	–	–	0.75	0.88	0.84
May and Mausbach ¹⁶	185	0.70–6.17	0.09–85.94	2.39	3.97	1.47	1.09	1.15	0.59	0.83
Grüneisen coefficient Γ										
Emampour <i>et al.</i> ⁹⁵	22	1.20–1.80	0.15–13.82	–	3.37	–	–	5.19	4.36	4.11
Mausbach and May ⁹⁶	191	0.70–6.17	0.09–98.13	1.41	0.53	3.11	0.33	0.43	0.38	0.48
Speed of sound w										
Lustig ¹⁷	8	1.01–3.00	0.20–8.22	–	–	2.89	–	0.21	0.05	0.80
May and Mausbach ¹⁶	191	0.70–6.17	0.09–85.94	1.47	2.77	2.06	0.17	0.63	0.28	0.45
Joule–Thomson coefficient μ_{JT}										
Lustig ¹⁷	7	1.01–3.00	0.20–8.22	–	–	3.98	–	5.59	2.15	3.39
May and Mausbach ¹⁶	170	0.70–6.17	0.09–85.94	3.52	6.73	3.65	2.86	4.02	1.52	2.29
Thermal expansion coefficient α										
Adams ³⁵	12	2.00–4.00	0.08–14.99	–	–	–	8.63	7.78	11.4	9.32
McDonald and Singer ⁷⁹	13	0.72–1.24	0.00–1.10	–	29.7	–	–	–	–	29.7
Isothermal compressibility β_T										
Adams ³⁵	12	2.00–4.00	0.08–14.99	–	–	–	7.34	7.98	12.1	9.09
Lotfi <i>et al.</i> ⁴²	5	0.75–1.30	0.00–0.12	–	2.01	28.6	–	–	–	7.33
May and Mausbach ¹⁶	188	0.70–6.17	0.09–98.13	2.48	1.19	6.40	1.11	1.49	0.79	1.10
McDonald and Singer ⁷⁹	15	0.72–1.24	0.00–1.10	–	17.1	–	–	–	–	17.1
Morsali <i>et al.</i> ⁸²	13	3.76	1.78–34.07	–	–	–	–	0.30	0.68	0.63
Thermal pressure coefficient γ										
Adams ³⁵	12	2.00–4.00	0.08–14.99	–	–	–	8.80	3.30	8.55	7.34
May and Mausbach ¹⁶	192	0.70–6.17	0.09–98.13	0.42	0.24	0.81	0.18	0.17	0.29	0.26
Meier ¹⁴	279	0.70–6.00	0.00–91.66	0.26	0.52	1.13	0.14	0.27	0.40	0.36
Morsali <i>et al.</i> ⁸²	13	3.76	1.78–34.07	–	–	–	–	0.11	0.20	0.18

density ρ'' . Ancillary correlations

$$\ln\left(\frac{p_v}{p_c}\right) = \left(\frac{T_c}{T}\right) \sum_{i=1}^5 n_i \left(1 - \frac{T}{T_c}\right)^{t_i}, \quad (44)$$

$$\frac{\rho'}{\rho_c} = 1 + \sum_{i=1}^5 n_i \left(1 - \frac{T}{T_c}\right)^{t_i}, \quad (45)$$

$$\ln\left(\frac{\rho''}{\rho_c}\right) = \sum_{i=1}^6 n_i \left(1 - \frac{T}{T_c}\right)^{t_i} \quad (46)$$

are included in the plots. Parameters are listed in Table 7. Ten different data sets are available for vapor pressure. The AAD are separated into three temperature ranges in Table 8. Molecular simulations were performed with different techniques and mostly low numbers of particles. The data of Adams^{36,63} ($N \approx 200$), Hansen and Verlet³⁸ ($N \approx 864$), Kofke⁶⁴ ($N \approx 108$ –256), Smit and Frenkel⁶⁵ ($N \approx 64$ –512), Panagiotopoulos⁶⁶ ($N \approx 300$ –500), and Panagiotopoulos *et al.*⁶⁷ ($N \approx 300$ –500) are represented with high deviations.

In particular, the vapor pressure data simulated by Panagiotopoulos⁶⁶ and Panagiotopoulos *et al.*⁶⁷ show a scatter of more than 20% and are not considered in the subsequent discussion. The data set best represented by the present equation of state was published by Lotfi *et al.*^{42,68} The NpT plus test particle method was used with 1372 particles in molecular dynamics mode. The results range from $T = 0.7$ to 1.3 with a scatter of 1.8% (AAD = 1.11%) relative to the present equation of state. Agrawal and Kofke⁴⁸ mainly investigated the solid-liquid and solid-vapor equilibrium. For the determination of the triple point, they simulated the crossing of the vapor-liquid equilibrium curve and the solid-liquid equilibrium curve. Vapor pressure data ($N \approx 108$) at low temperatures show a systematic deviation of -3.5% . This trend is in agreement with other data sets for $T < 0.75$, e.g., Lotfi *et al.*⁴² However, modeling the vapor pressure curve such that it reproduces these data would require an unreasonable course of the saturation line, so they are assumed to be inaccurate. The present EOS is in good agreement with the EOS of Mecke *et al.*⁵ at low temperatures. Since the data set of Lotfi *et al.*⁴² is the most consistent and accurate one, the corresponding scatter of 1.8% was assumed to be the uncertainty in vapor pressure.

The saturated liquid density was investigated by 14 different authors. The relative deviation with respect to the present equation of state is illustrated in Fig. 14. Most of the data were taken from the same publications as the vapor pressures. Therefore, the underlying molecular simulation conditions are the same. Data scatter less and the representation of the data is much better. For $T < 1.1$, the data of Adams³⁶ (AAD = 0.52%–0.92%), Hansen and Verlet³⁸ (AAD = 0.15%–0.48%), Panagiotopoulos⁶⁶ (AAD = 0.13%–1.08%), Panagiotopoulos *et al.*⁶⁷ (AAD = 0.25%–1.00%), Martin and Siepmann⁶⁹ (AAD = 0.30%–0.40%), Smit and Frenkel⁶⁵ (AAD = 0.81%), Potoff and Panagiotopoulos⁷⁰ (AAD = 0.93%), and Kofke⁶⁴ (AAD = 0.74%) are represented within 1%. The data of Agrawal and Kofke⁴⁸ deviate systematically by 1.4% and were not considered further. Again, the most consistent and accurate data set is by Lotfi *et al.*⁴² (AAD = 0.03%–0.14%). For $T \geq 1.1$, two different observations are made. The data of Kofke,⁶⁴ Shi and Johnson,⁷¹ and Hunter and Reinhardt⁷² yield higher densities than the present EOS. The data of Kofke⁶⁴ are inaccurate in the lower temperature range. Shi and Johnson⁷¹ published consistent data within a small temperature range ($T = 1.15$ – 1.27). The present EOS predicts these data within 0.7%, except for the data point at the highest temperature, which is off by 1.5%. The data of Hunter and Reinhardt⁷² exhibit significant scatter, which is probably due to varying numbers of particles ($N = 32$ – 500) used in their simulations. Relative to the present EOS, the data by Potoff and Panagiotopoulos⁷⁰ deviate by up to -2.7% . These data support the data of Lotfi *et al.*⁴² at temperatures close to T_c . Since no vapor-liquid equilibrium data were used in the fit, the present EOS independently supports that the data of Lotfi *et al.*⁴² are accurate over the entire temperature range. The uncertainty of saturated liquid density calculated with the present EOS is assumed to be 0.15% for $T < 1.1$ and 0.5% for $T \geq 1.1$ based on the data of Lotfi *et al.*⁴²

Finally, the relative deviation of directly simulated saturated vapor density data from the present EOS is plotted in Fig. 14. The available data are from the same sources. The representation of the data is similar to the vapor pressure and is not discussed further. Again, the data set of Lotfi *et al.*⁴² as a reference yields a correlation uncertainty of 1.8% over the entire temperature range.

5.4. Density at homogeneous states

It is common for equation of state correlations for real fluids to quote deviations for density at given temperature and pressure. We adopt the tradition, although it was outlined recently that for molecular simulation data the procedure is not necessary.⁷⁵ The homogeneous density and the residual internal energy are described equally well by the present EOS and that of Mecke *et al.*⁵ The average absolute relative

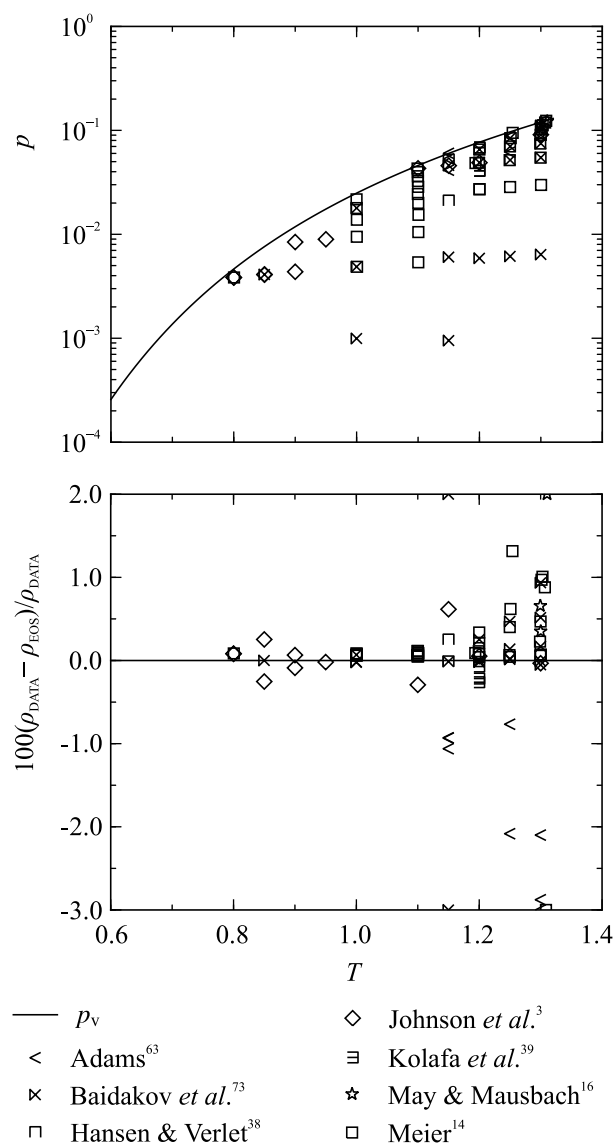


FIG. 15. Representation of vapor-phase density data. Top: Simulated state points relative to the vapor pressure curve. Bottom: Relative deviation of the simulated gas density data from the present equation of state.

deviations for literature data are listed in Table 9. The gas phase was studied by seven independent authors. Figure 15 shows comparisons of density data in the gaseous region with the present EOS. Apparently, the most accurate data were published by Johnson *et al.*³ (AAD = 0.17%), Kolafa *et al.*³⁹ (AAD = 0.19%), and Meier¹⁴ (AAD = 0.33%). All are

represented by the present EOS within 1%, which validates the description of the vapor phase up to the saturated vapor line. The homogeneous liquid phase was investigated more comprehensively than the gas phase. In total, 26 different data sets are available, which are presented in Fig. 16. In contrast to the gas-phase data, the liquid-phase data are predominantly far

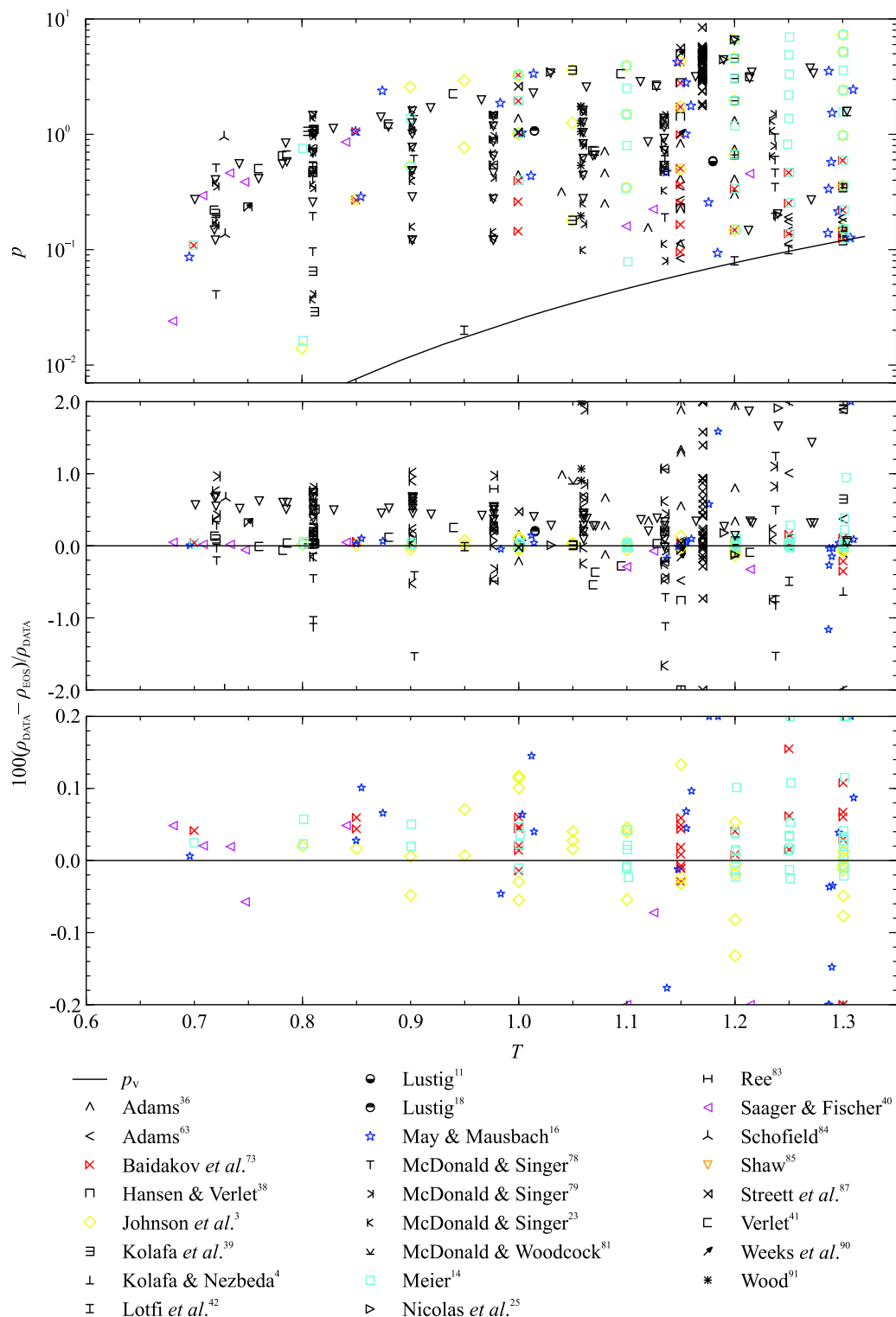


FIG. 16. (Color online) Representation of liquid-phase density data. Top: Simulated state points relative to the vapor pressure curve. Center: Relative deviation of all available simulated data from the present equation of state. Bottom: Relative deviation of selected simulated data from the present equation of state.

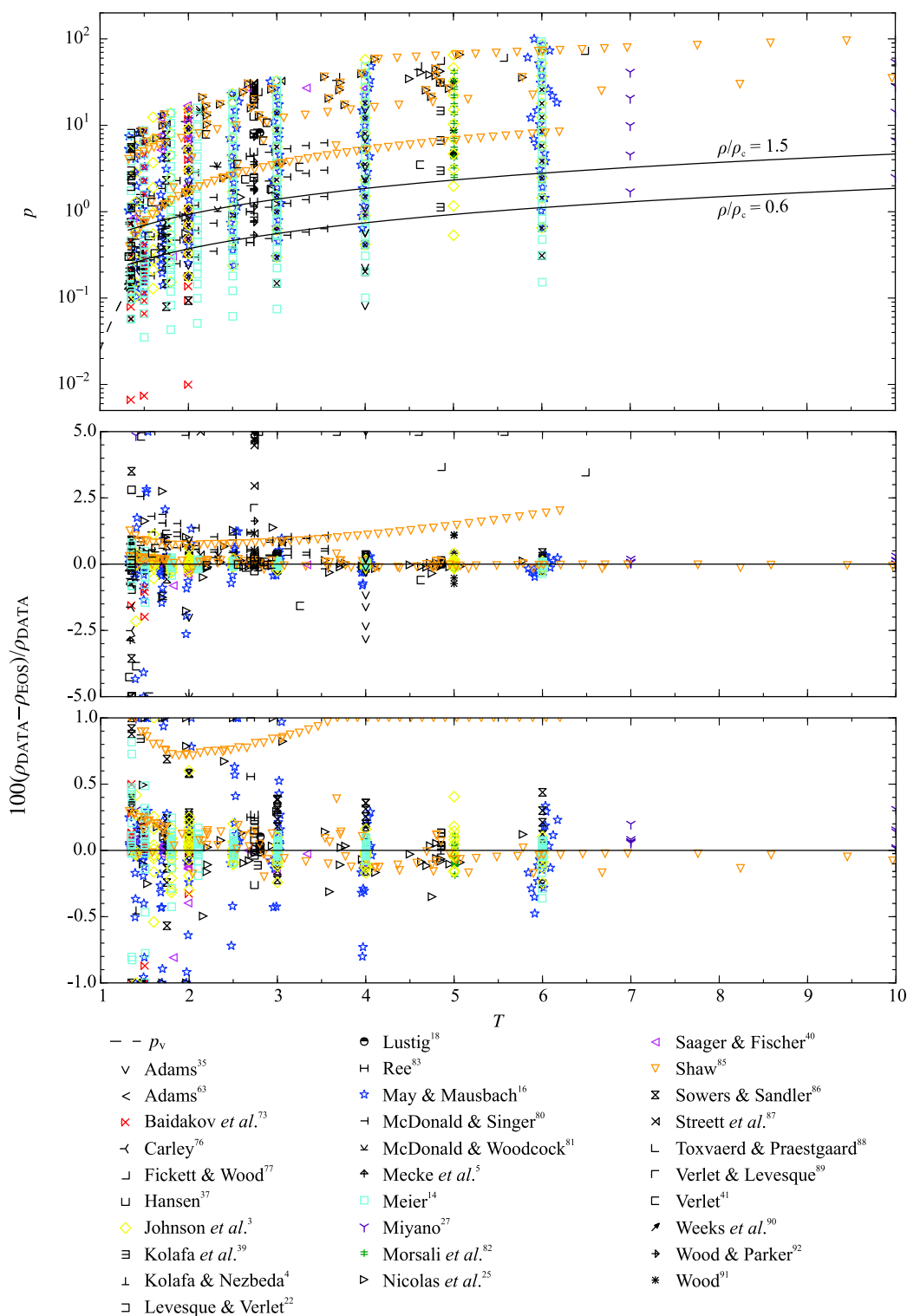


FIG. 17. (Color online) Representation of density in the supercritical region. Top: p – T diagram of state points. Center: Relative deviation of all available simulation data from the present equation of state. Bottom: Relative deviation of selected simulation data from the present equation of state.

away from the two-phase region. When fitting an equation of state based on such data, as Mecke *et al.*⁵ did, saturated liquid density data would be helpful. Thus, Mecke *et al.*⁵ applied VLE data to their fit, which was not done here. Keeping in mind that the representation of VLE data is similar for both equations, the strategy of fitting only data at homogeneous states together

with virial coefficients for the gas phase compensates for a lack of VLE data as long as the homogeneous data are close enough to the two-phase region. This is particularly true if derivatives of the Helmholtz energy are considered directly.

Some of the literature data appear to be of poor quality, so only the most accurate and comprehensive data sets^{3,14,16,40,73,85}

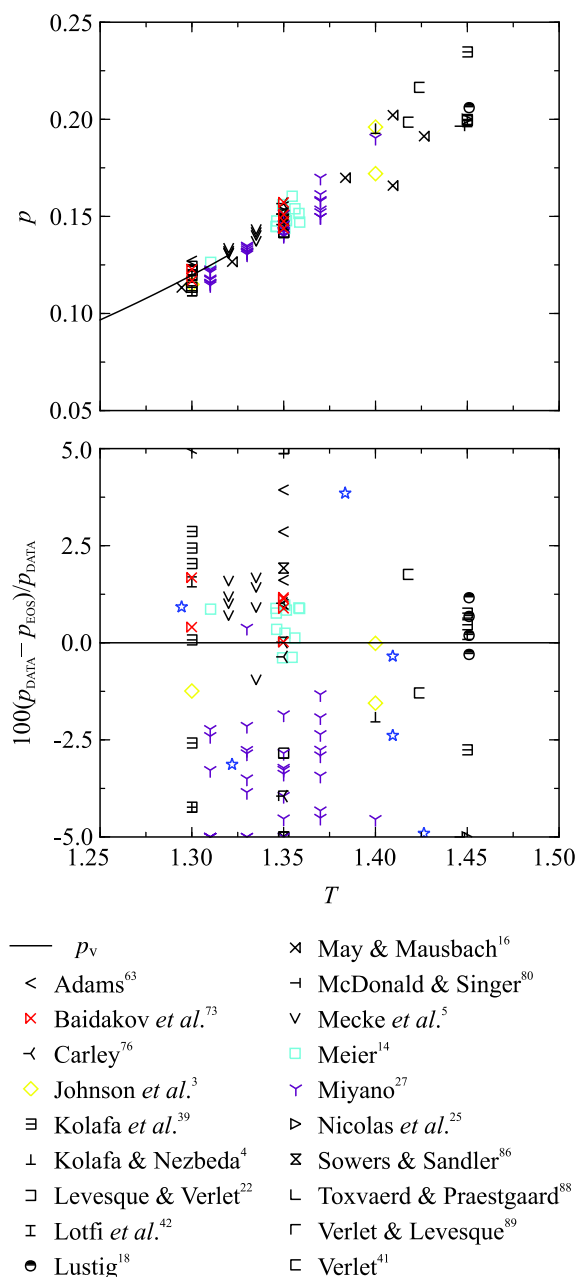


FIG. 18. (Color online) Representation of literature data for pressure in the critical region. Top: p - T diagram showing the distribution of the state points relative to the vapor pressure curve. Bottom: Relative deviation of the simulated pressure data from the present equation of state in the critical region.

(colored symbols in Fig. 16) are considered for the assessment of uncertainty. The most accurate data are Johnson *et al.*³ (AAD = 0.05%), Meier¹⁴ (AAD = 0.07%), and Baidakov *et al.*⁷³ (AAD = 0.06%). The high AAD of 0.35% of May and Mausbach¹⁶ is caused by a few data points near the critical temperature. If those points are excluded, the data set of May and Mausbach¹⁶ is represented as well as the data sets above. For all data, deviations increase with increasing temperature. The lower temperature region ($T < 1.1$) is modeled with an uncertainty of 0.06%. The upper temperature region is reproduced within 0.1%, with slightly higher deviations near the

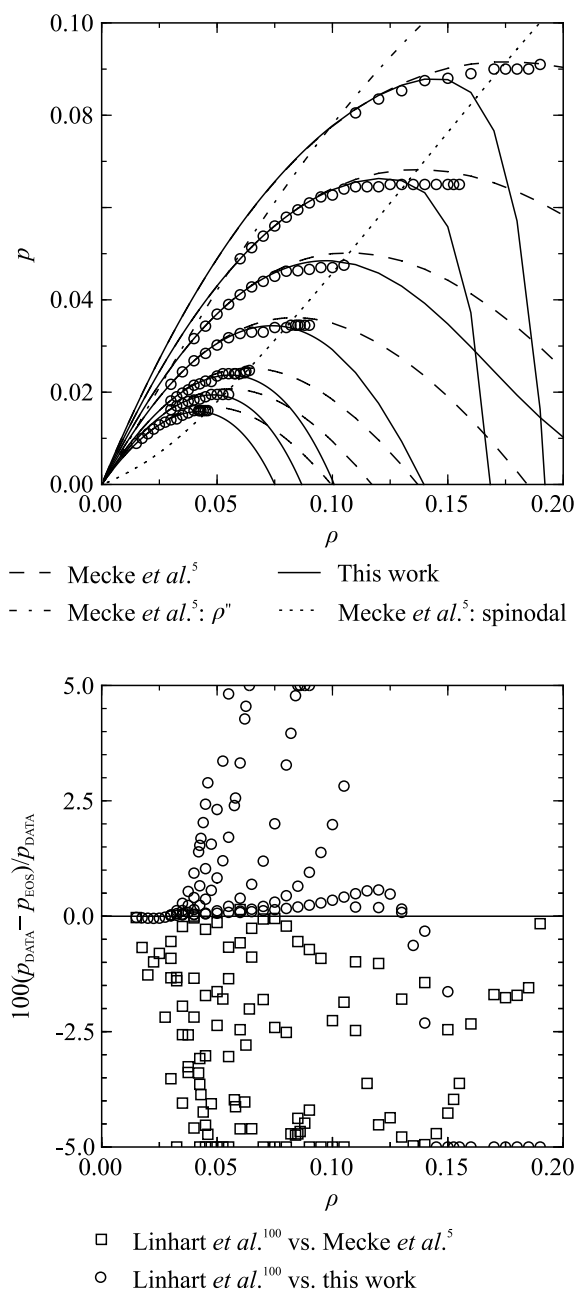


FIG. 19. Comparison of metastable gaseous pressure data of Linhart *et al.*¹⁰⁰. The EOS of Mecke *et al.*⁵ is shown for comparison. Top: p - ρ diagram with selected isotherms and the spinodal corresponding to the equation of Mecke *et al.*⁵. Bottom: Relative deviation of the metastable pressure data of Linhart *et al.*¹⁰⁰ from the present equation of state (open circles) and that of Mecke *et al.*⁵ (open squares).

critical temperature. The uncertainty of the present EOS is estimated to be 0.1% in the entire liquid region.

Similar to Table 5, the average absolute relative deviation for density at supercritical states, as listed in Table 9, is separated into three density ranges and investigated up to $T = 7$ ($T/T_c = 5.3$). For the HD region, higher temperatures are available ($T_{\text{max}} = 136$ or $T_{\text{max}}/T_c \approx 100$). In total, 25 data sets with a maximum pressure of approximately $p_{\text{max}} = 190$ ($p_{\text{max}}/p_c \approx 1460$) are published. For orientation, the range of validity of typical fluid equations of state for real substances

is significantly smaller, e.g., $T_{\max}/T_c \approx 13$ and $p_{\max}/p_c \approx 210$ for argon,⁶⁰ $T_{\max}/T_c \approx 6.5$ and $p_{\max}/p_c \approx 110$ for carbon dioxide,⁹⁷ and $T_{\max}/T_c \approx 15$ and $p_{\max}/p_c \approx 650$ for nitrogen.⁹⁸ The most accurate and comprehensive data sets^{3,14,16,40,73,82,85} are plotted as colored symbols and presented at the bottom of Fig. 17. The data of May and Mausbach¹⁶ show relatively large scatter, so they were excluded from the uncertainty analysis. Data in the low-density region ($\rho < 0.217$) by Johnson *et al.*³ (AAD = 0.14%), Meier¹⁴ (AAD = 0.11%), and Baidakov *et al.*⁷³ (AAD = 0.08%) are reproduced best. Based on these data sets, the estimated uncertainty in density as a function of temperature and pressure of the present EOS is 0.15%. Data in the medium-density range ($0.217 \leq \rho \leq 0.434$) by Lustig¹⁷ (AAD = 0.03%), Meier¹⁴ (AAD = 0.21%), Kolafa *et al.*³⁹ (AAD = 0.09%), and Morsali *et al.*⁸²

(AAD = 0.04%) agree best with the present equation. The data of Johnson *et al.*³ are also represented well, with an AAD of 0.28% attributed to two outliers with deviations of 1% and 2%. Based on these five data sets, the estimated uncertainty in density of the present EOS is assumed to be 0.3% in the medium-density range. The high-density range was accurately simulated by Johnson *et al.*³ (AAD = 0.08%), Lustig¹⁷ (AAD = 0.03%), Meier¹⁴ (AAD = 0.05%), Saager and Fischer⁴⁰ (AAD = 0.08%), Baidakov *et al.*⁷³ (AAD = 0.04%), and Morsali *et al.*⁸² (AAD = 0.08%). Based on comparisons with these data, the uncertainty of the present EOS in the high-density region is estimated as 0.2% in density.

Throughout, the uncertainty estimates are higher in the vicinity of the critical point. The critical region was not intended to be modeled as accurately as the remaining fluid region, for

TABLE 10. Critical parameters of the Lennard-Jones fluid from the literature

Authors	Year	T_c	ρ_c	p_c
Adams ⁶³	1979	1.30(2)	0.33(3)	0.13(2)
Adams <i>et al.</i> ¹⁰⁷	1979	1.30(2)	0.33(3)	—
Amadei <i>et al.</i> ¹⁰⁸	1999	1.350	0.337	0.149
Barker <i>et al.</i> ²⁹	1966	1.291	0.547	0.249
		1.449	0.771	0.379
		1.300	0.561	0.249
Caillol ¹⁰²	1998	1.326(2)	0.316(2)	0.111(2)
Dunikov <i>et al.</i> ¹⁰¹	2001	1.350(5)	0.310(5)	0.126(8)
Hess ¹⁰³	1999	1.28	0.25	0.1056
		1.41	0.29	0.1472
		1.33	0.3	0.1357
Hunter and Reinhardt ⁷²	1995	1.32	—	—
Johnson <i>et al.</i> ³	1993	1.313	0.310	—
Kim <i>et al.</i> ¹⁰⁹	1969	1.35	0.30	0.14
		1.28	0.29	0.13
Kofke ^{64,110}	1993	1.324(12)	0.305(2)	—
		1.321(4)	0.306(1)	—
Kolafa and Nezbeda ⁴	1994	1.3396	0.3108	0.1405
Koutras <i>et al.</i> ¹¹¹	1992	1.355	0.290	0.147
Levesque and Verlet ²²	1969	1.37	0.31	0.140288
		1.36	0.36	0.151776
		1.36	0.33	0.161568
Lotfi <i>et al.</i> ⁴²	1992	1.31	0.314	—
Martin and Siepmann ⁶⁹	1998	1.2921	0.3117	0.1144
May and Mausbach ³⁰	2012	1.3145	0.3107	—
Mecke <i>et al.</i> ⁵	1996	1.328	0.3107	—
Miyano ²⁷	1993	1.35	0.32	0.142
Nicolas <i>et al.</i> ²⁵	1979	1.35	0.35	0.142
Panagiotopoulos ⁶⁶	1987	<1.35	0.31(2)	—
Potoff and	1998	1.312(7)	0.316(1)	0.1279(6)
Panagiotopoulos ¹⁰⁴				
Potoff and	2000	1.312(7)	0.316(2)	—
Panagiotopoulos ⁷⁰				
Ree ⁸³	1980	1.41	0.33	0.177
Shi and Johnson ⁷¹	2001	1.3241(9)	0.3165(7)	—
		1.3145(2)	0.316(1)	—
Smit ¹⁰⁵	1992	1.316(6)	0.304(6)	—
Song and Mason ²⁴	1989	1.306	0.2625	0.1225
Sowers and Sandler ⁸⁶	1991	1.372	0.313	0.156
Sung and Chandler ¹⁰⁶	1974	1.3103	0.318	0.121
		1.31(1)	0.33(3)	—
Sýs and Malijevský ¹¹²	1980	1.35	0.33	0.147
Valleau ³²	1994	1.328(3)	—	—
Verlet and Levesque ⁸⁹	1967	1.26	0.297	0.316
Verlet ⁴¹	1967	1.36(4)	0.31(3)	—

several reasons. Natural large-scale fluctuations of a fluid in the critical region make sampling of some thermodynamic properties particularly difficult and uncertain. Molecular simulation results may cause a curvature in the rectilinear diameter⁹⁹ at high reduced temperatures when fitting an equation of state to them. That was observed for several different fluids, e.g., benzene, cyclohexane, and hydrogen sulfide, and is presented by Thol *et al.*⁶² for the Lennard-Jones fluid truncated and shifted at 2.5σ . During fitting iterations of the present EOS for the Lennard-Jones fluid, the nonlinearity of the rectilinear diameter was minimized. Available data are presented in Fig. 18. Some of the simulation data have higher deviations in the critical region than elsewhere. Again, the data of Mecke *et al.*,⁵ Lustig,¹⁷ Meier,¹⁴ and Baidakov *et al.*⁷³ appear to be the most accurate in the critical region. The uncertainty in this region is 2% in pressure.

In Fig. 19, a comparison of the gaseous metastable pressure data published by Linhart *et al.*¹⁰⁰ with the present equation of state is shown. In the top panel, a $p - \rho$ diagram including the saturated vapor line, the spinodal, and the simulated data along the corresponding isotherms is presented. A reasonable trend of the data is observed for densities $\rho \leq \rho_{\text{spinodal}}$. In this region, slopes and curvatures of isotherms of the present EOS are in better agreement with the data than the EOS of Mecke *et al.*,⁵ which is confirmed by the deviation plot on the bottom panel of Fig. 19. For $\rho < 0.15$, the deviations between the present EOS and the simulation data are much lower than those of

Mecke *et al.*⁵ Therefore, the qualitative validity of the present EOS extends into the metastable region up to the gaseous spinodal.

5.5. Critical point

The critical point is central for the development of a fluid equation of state. In this work, as in Thol *et al.*⁶² and Lustig *et al.*,⁷⁵ we did not impose a critical point. The critical temperature and density varied during the fitting procedure. In particular, the modeling of an almost linear rectilinear diameter and the shaping of a distinctive saddle point of the critical isotherm was carefully monitored during the fit to ensure that the critical values did not exceed the uncertainties of the data given in the literature. Table 10 presents critical parameters from the literature, and the most likely critical points are illustrated in Fig. 20. The critical density that was observed during the fit of the present equation of state ($\rho_c = 0.31$) is in line with the average critical density from the literature. It is in good agreement with the critical density of Dunikov *et al.*,¹⁰¹ Johnson *et al.*,³ Kolafa and Nezbeda,⁴ Martin and Siepmann,⁶⁹ Mecke *et al.*,⁵ Miyano,²⁷ and Verlet.⁴¹ For the critical temperature, the main values scatter around $T_c = 1.35$. The corresponding critical density data show significant scatter. Therefore, the critical temperature values around $T_c = 1.32$ seem to be a more adequate basis for comparison. The critical temperature obtained from the present EOS is in good agreement with

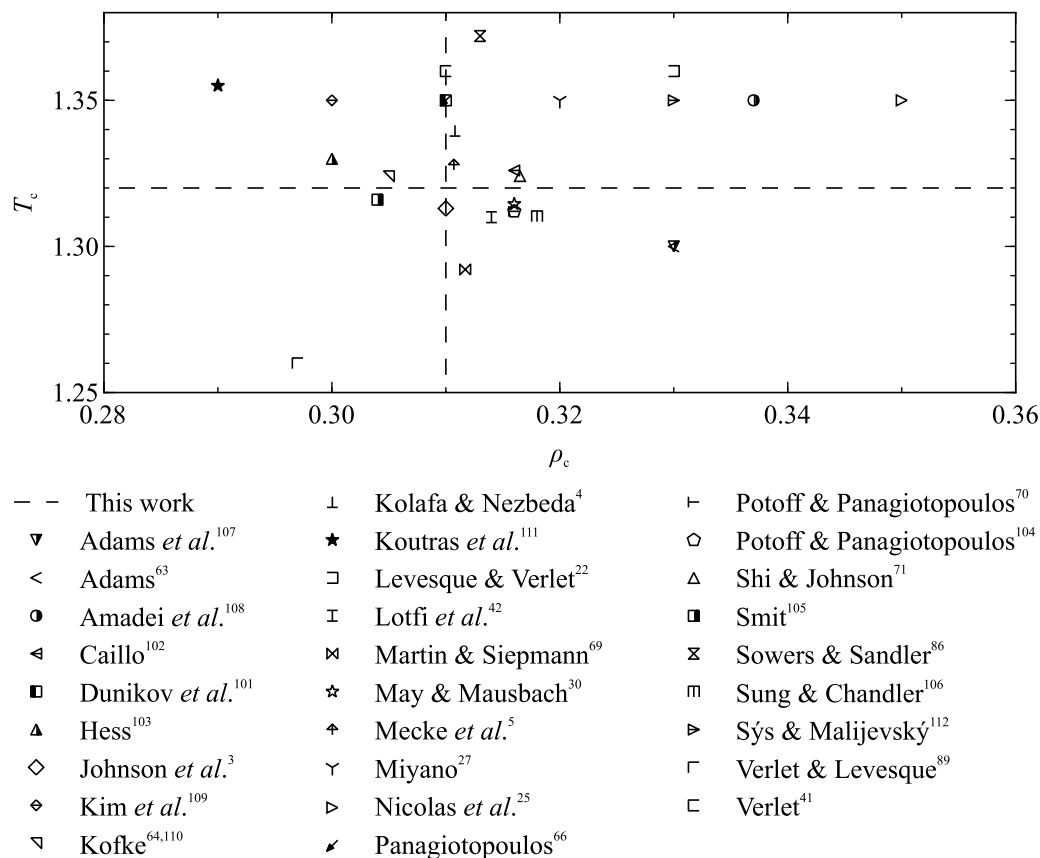


Fig. 20. Selected critical parameters from the literature. The crossing of the two dashed lines denotes the critical point of this work ($T_c = 1.32$, $\rho_c = 0.31$).

Caillol,¹⁰² Hess,¹⁰³ Johnson *et al.*,³ Kofke,⁶⁴ Lotfi *et al.*,⁴² Mecke *et al.*,⁵ Potoff and Panagiotopoulos,^{70,104} Shi and Johnson,⁷¹ Smit,¹⁰⁵ and Sung and Chandler.¹⁰⁶ Thus, the critical temperature $T_c = 1.32$ and the critical density $\rho_c = 0.31$ were applied to the present equation (cf. calculation of τ and δ in Eq. (2)). The critical pressure $p_c \approx 0.130\,06$ is calculated as a function of the critical temperature and density in this work.

5.6. Caloric properties

The residual internal energy was investigated to the same extent as the ppT data. The average absolute relative deviations of the data of each author are listed in Table 9. The data sets assumed to be most accurate were pointed out in the density discussion. Since density and residual internal energy

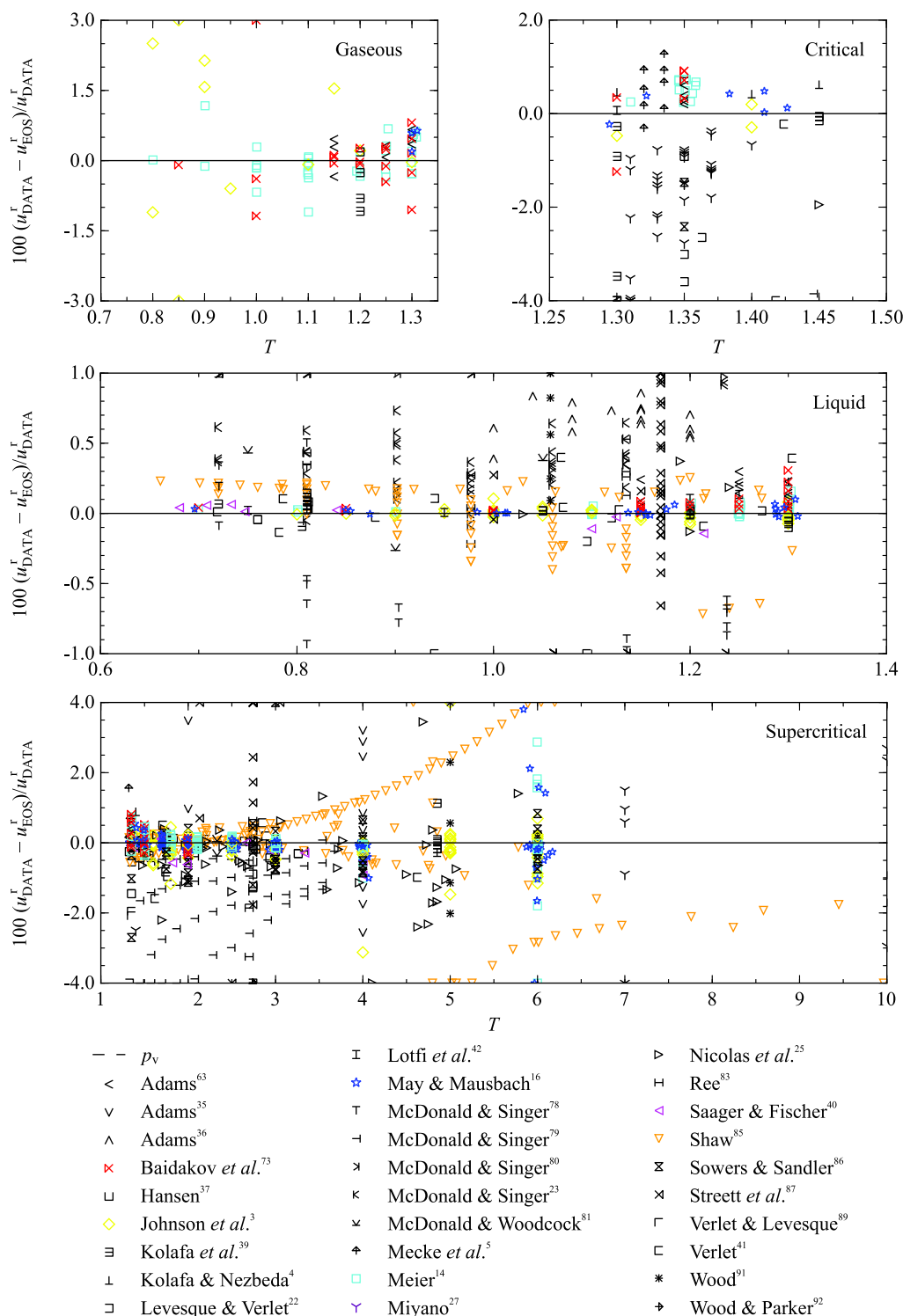


FIG. 21. (Color online) Relative deviation of literature data for residual internal energy from the present equation of state. Separate plots are provided for the gaseous, critical, liquid, and supercritical region.

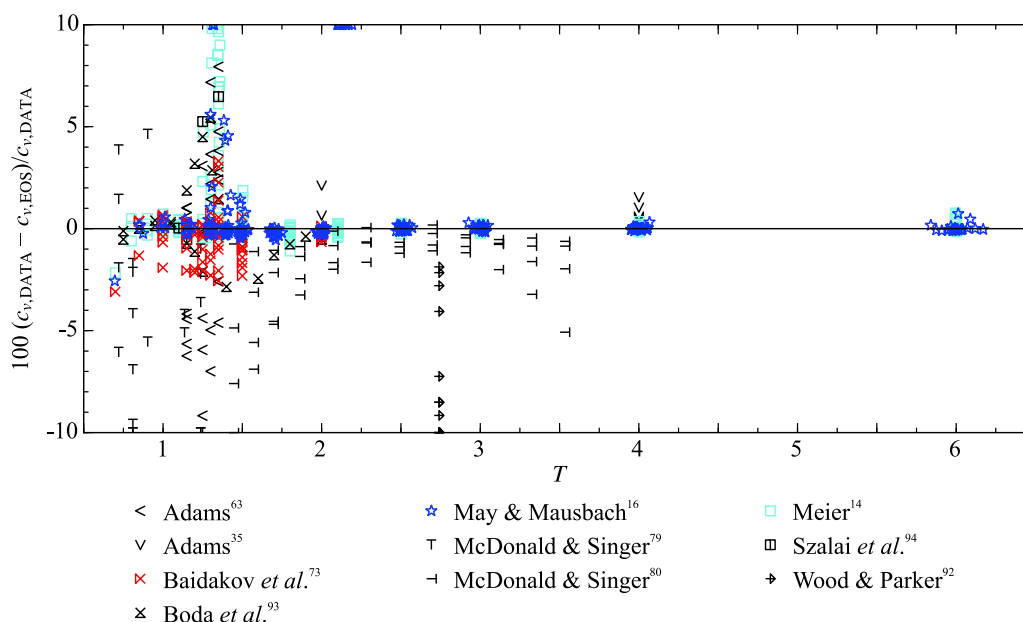


FIG. 22. (Color online) Relative deviation of literature data for isochoric heat capacity from the present equation of state.

are from the same molecular simulation runs, the quality of the data should be similar. Only data colored as for density in Figs. 16 and 17 are discussed.^{3,14,16,40,73,85} Figure 21 presents the relative deviation of simulated residual internal energy data from calculated values. In the gaseous region, Meier¹⁴ ($AAD = 0.30\%$) and Baidakov *et al.*⁷³ ($AAD = 0.70\%$) are represented by the present equation best. Based on these data, the uncertainty of the present EOS is estimated to be 1% in the gaseous region. In the liquid phase, the new equation is in agreement with the data of Johnson *et al.*³ ($AAD = 0.03\%$), Meier¹⁴ ($AAD = 0.02\%$), May and Mausbach¹⁶ ($AAD = 0.02\%$), and Baidakov *et al.*⁷³ ($AAD = 0.06\%$). The uncertainty of the residual internal energy calculated with the present EOS is determined to be 0.1% in the liquid region. The uncertainty in the critical region is estimated to be 1%, which is supported by Johnson *et al.*³ ($AAD = 0.32\%$), May and Mausbach¹⁶ ($AAD = 0.28\%$), Meier¹⁴ ($AAD = 0.53\%$), and Baidakov *et al.*⁷³ ($AAD = 0.74\%$). The supercritical region is well described up to $T = 7$ in agreement with the density results. Data of Johnson *et al.*³ ($AAD = 0.21\%–0.34\%$), Meier¹⁴ ($AAD = 0.15\%–0.27\%$), May and Mausbach¹⁶ ($AAD = 0.13\%–0.26\%$), and Baidakov *et al.*⁷³ ($AAD = 0.05\%–0.27\%$) scatter within 1% of the present EOS, which is assumed to be the uncertainty of the equation.

Only the data set of Lotfi *et al.*⁴² is available for the residual enthalpy. The simulations were carried out along the saturation curves (see supplementary material⁵²). The saturated liquid line is described within 0.1% for $T \leq 1$ and 0.5% for $T > 1$. The simulations of the saturated vapor phase scatter around the equation by 4%.

In the homogeneous region, isochoric heat capacity data of Meier¹⁴ and May and Mausbach¹⁶ are represented best by the present equation (cf. Fig. 22 and Table 9). Except for the critical region, these data agree within 0.5%. Compared to the equation of Mecke *et al.*,⁵ the representation of the data

published by Meier¹⁴ in the vapor phase ($AAD = 0.40\%$ vs. $AAD_{Mecke} = 1.21\%$) and in the critical region ($AAD = 3.09\%$ vs. $AAD_{Mecke} = 7.49\%$) are improved significantly. The data of May and Mausbach¹⁶ are reproduced better than those of Meier.¹⁴ Deviations in the critical region increase to 5%. Only one data set⁹³ was simulated along the saturation lines. For $T \leq 1.2$, the data scatter within 0.5% around the present equation, which is within statistical uncertainties. For higher temperatures, the deviations increase significantly. In the low-temperature region of the $c_v - T$ diagram in Fig. 23, the present EOS and that of Mecke *et al.*⁵ show agreement with the data of Boda *et al.*⁹³ Only at $T = 0.75$, the equation of Mecke *et al.*⁵ overestimates the saturated liquid isochoric heat capacity, which yields a steeper increase of the saturation line when extrapolated to low temperatures. Therefore, additional simulations were carried out in this work to show that the trend of the present EOS is correct. At $T = 1.2$, the saturated liquid and vapor isochoric heat capacities approach the same value and then cross each other. This is perfectly modeled by the

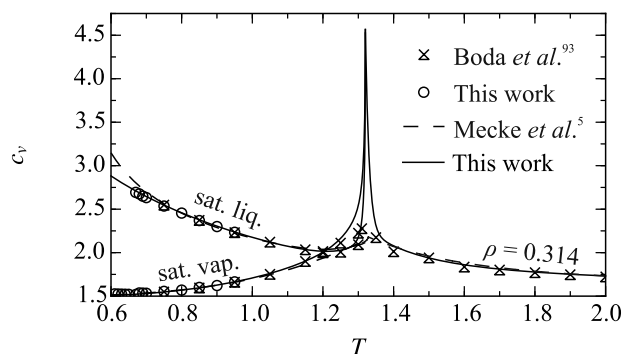


FIG. 23. Isochoric heat capacity versus temperature. The saturated liquid and vapor lines calculated with the equation of Mecke *et al.*⁵ are plotted for comparison.

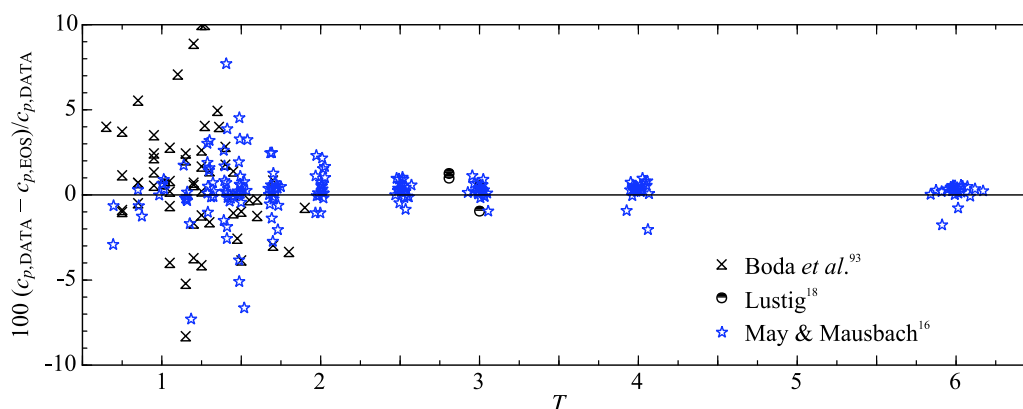


Fig. 24. (Color online) Relative deviation of literature data for isobaric heat capacity from the present equation of state.

present EOS, while the crossing of the equation of Mecke *et al.*⁵ is shifted to about $T = 1.275$. At $T > 1.2$, high deviations of the present EOS from the isochoric heat capacity data of Boda *et al.*⁹³ are caused by a lower curvature of the simulation data. Large-scale fluctuations in the critical region make sampling of heat capacities difficult. While a classical equation of state cannot reproduce the correct physical behavior for isochoric heat capacity (a weak divergence toward infinity), our EOS at least produces a steep maximum in this property upon approaching the critical point.

The isobaric heat capacity was investigated by three authors. Figure 24 shows relative deviations of the simulation data and the present equation of state. The data of May and Mausbach¹⁶ are represented within 1%, which is estimated to be the uncertainty of the EOS outside of the critical region. In contrast to the isochoric heat capacity, the isobaric heat capacity data of Boda *et al.*⁹³ show a significant scatter of approximately 5%–10%. These data are investigated in more detail in Fig. 25. Similar to the isochoric heat capacity, the present EOS exhibits a steeper increase of the saturated isobaric heat capacity approaching the critical temperature than that of Mecke *et al.*⁵

Figure 26 presents data for the Grüneisen coefficient Γ . Historically, this property was not utilized in the context of

fluid equations of state. Introduced for fluids by Arp *et al.*,¹¹³ it was found to be valuable for the development of EOS in recent years, e.g., for the truncated and shifted Lennard-Jones fluid,⁶² ethylene oxide,¹¹⁴ hexamethyldisiloxane,¹¹⁵ R1234ze(E),¹¹⁶ R245fa,¹¹⁷ cyclopentane,¹¹⁸ and cyclohexane.¹¹⁹ It is defined as the thermal pressure coefficient divided by the density and the isochoric heat capacity (Eq. (24)) and establishes a connection between thermal and caloric thermodynamic properties. The behavior of the speed of sound and the isochoric heat capacity can be monitored simultaneously by the Grüneisen coefficient. Thus, while it is not important for practical tasks, it is useful for verifying correct behavior of equations of state. In Fig. 26, a Γ - ρ diagram and relative deviations of simulated Grüneisen coefficient data from calculated values are depicted. The isotherms show an increasing Grüneisen coefficient with increasing density. Similar to values calculated from many EOS for real fluids (e.g., nitrogen,⁹⁸ benzene,¹²⁰ argon,⁶⁰ and carbon dioxide⁹⁷), a crossing of isotherms occurs near the critical density. This behavior is assumed to be correct because it was found for several different fluids. No direct experimental measurements are available for the Grüneisen coefficient to verify these assumptions. Therefore, Emampour *et al.*⁹⁵ and Mausbach and May⁹⁶ are important publications providing Grüneisen coefficient data from molecular

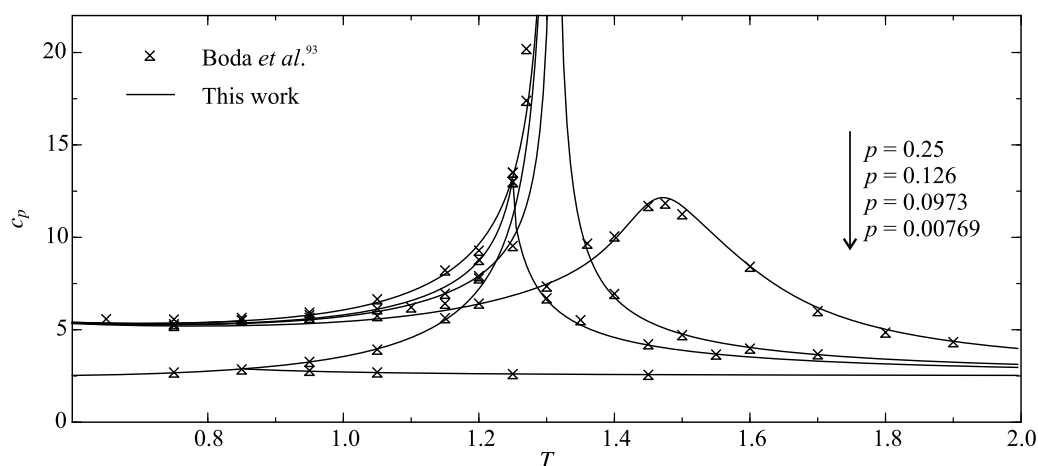


Fig. 25. Isobaric heat capacity versus temperature along isobars.

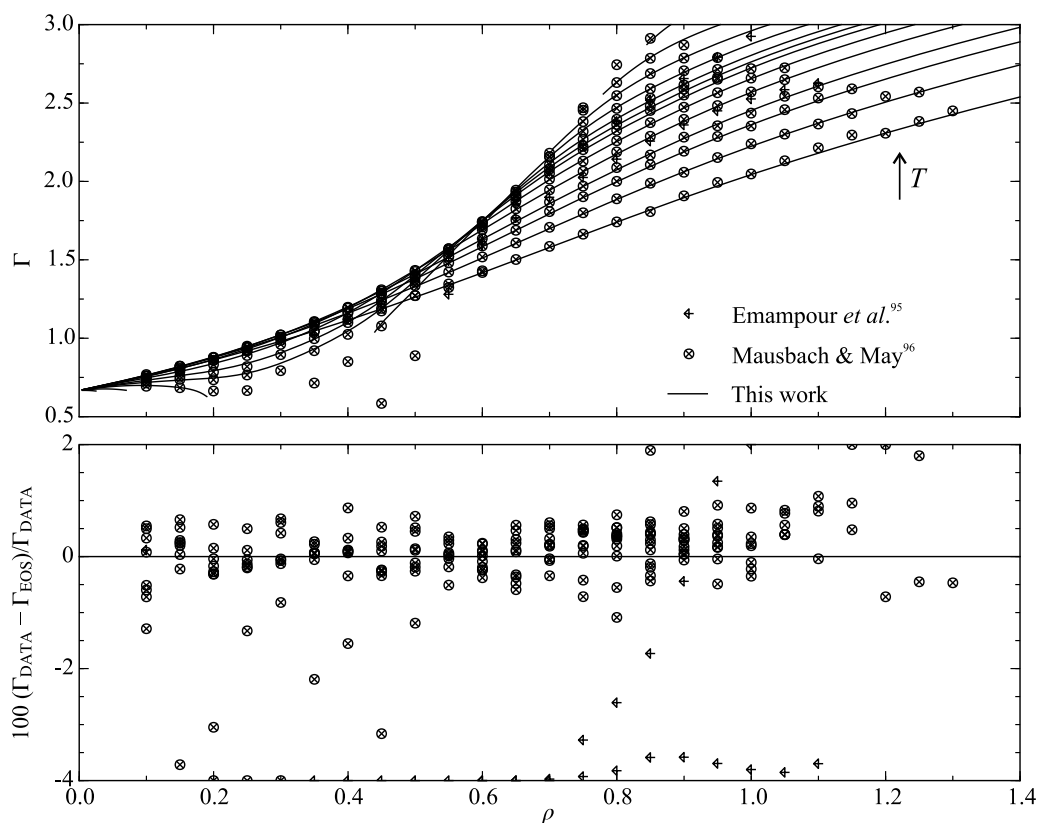


FIG. 26. Comparison of literature data for the Grüneisen coefficient with the present equation of state. Top: Γ - ρ diagram along isotherms. Bottom: Relative deviation of simulated Grüneisen coefficient data from the present equation of state.

simulation. Mausbach and May⁹⁶ in particular carried out a comprehensive investigation of the Grüneisen coefficient over a broad range of temperature and density. At least for the Lennard-Jones fluid, they could prove the presumed behavior to be correct. The present EOS follows the trend of the molecular simulation data and the deviation between simulated and calculated data is mostly within 1.5%. The uncertainty increases in the critical region. The simulations of Mausbach and May⁹⁶ were carried out in the *NVE* ensemble, where temperature is not an input but measured. Thus, the simulation data slightly scatter around isotherms. However, for the uncertainty

calculation, the measured temperatures of the simulation data were used. The data of Emampour *et al.*⁹⁵ were not considered in the uncertainty estimate because they show a systematic negative offset relative to both the data of Mausbach and May⁹⁶ and the present EOS.

The speed of sound has not been thoroughly investigated with molecular simulation. Two different data sets are available: May and Mausbach¹⁶ and Lustig.¹⁷ Figure 27 shows relative deviations between the present EOS and the simulation data of about 1%. The uncertainty increases in the vicinity of the critical point.

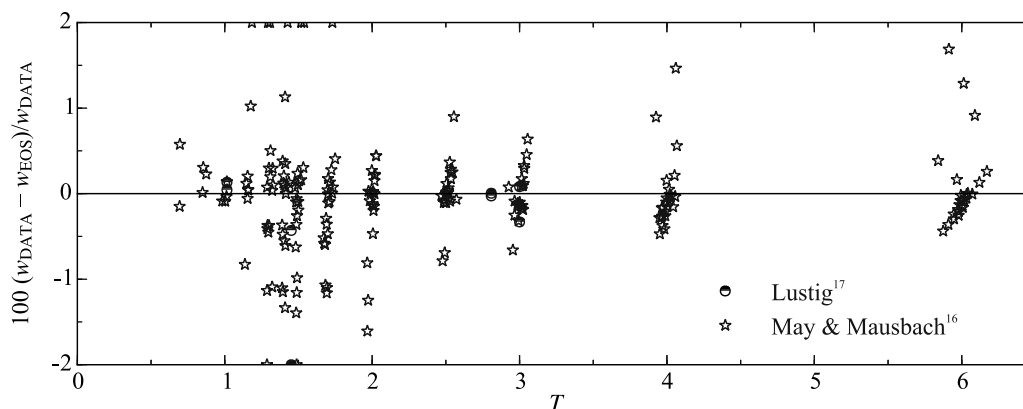


FIG. 27. Relative deviation of literature data for speed of sound from the present equation of state.

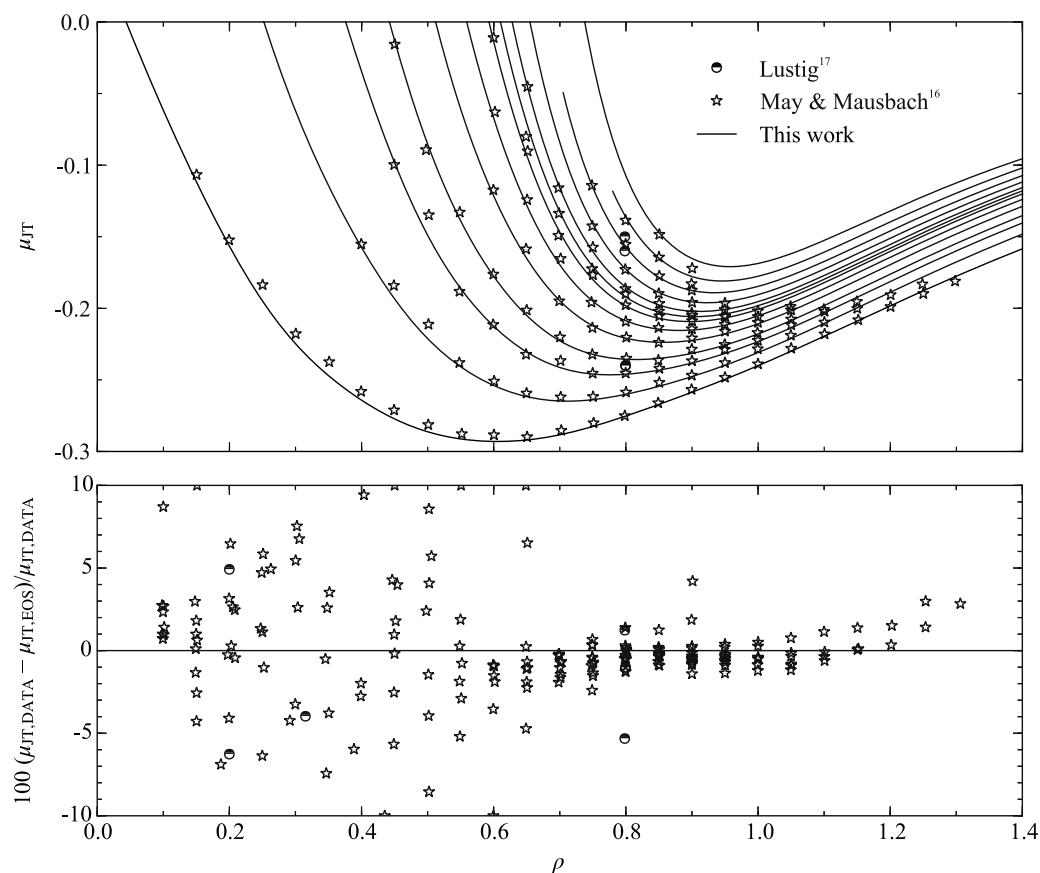


FIG. 28. Comparison of literature data for the Joule–Thomson coefficient with the present equation of state. Top: Joule–Thomson coefficient versus density along isotherms. Bottom: Relative deviation of simulated Joule–Thomson coefficient data from the present equation of state.

The Joule–Thomson coefficient μ_{JT} was investigated by Lustig¹⁷ and by May and Mausbach.¹⁶ The top panel of Fig. 28 presents a μ_{JT} – ρ diagram with selected isotherms. Over the entire temperature and density range, slopes and curvatures of the present equation of state agree well with the simulation results. The uncertainty for calculated Joule–Thomson coefficient data using the present EOS is estimated to be 2.5% over the entire temperature range and for densities $\rho \geq 0.6$. Lower densities go along with larger deviations, which leads to an uncertainty of up to 10%.

The thermal expansion coefficient $\alpha = 1/v(\partial v/\partial T)_p$, the isothermal compressibility $\beta_T = 1/(\rho(\partial p/\partial \rho)_T)$, and the thermal pressure coefficient $\gamma = (\partial p/\partial T)_\rho$ are illustrated in Fig. 29. The thermal expansion coefficient was investigated by Adams,³⁵ McDonald and Singer,⁷⁹ and Boda *et al.*⁹³ Depending on the location on the fluid surface, it is extremely sensitive to the course of isobars in the ρ – T diagram. Wagner and Thol¹²¹ have shown for water that it is possible to have huge deviations in α although densities are modeled precisely. Therefore, simulations must be carried out very accurately. New simulations were carried out in this work, which are accurate to within 5% when comparing to the present EOS. The isothermal compressibility and the thermal pressure coefficient are easier to correlate. Reliable data of Meier¹⁴ and May and Mausbach¹⁶ are available for these properties. Calculated data on isothermal compressibility are uncertain by 3% and on pressure coefficient are uncertain by 1%.

5.7. Physical behavior and extrapolation

In addition to a comprehensive analysis of thermodynamic properties that are available in the literature, the extrapolation behavior and physical trends of several different properties must be monitored when setting up fundamental equations of state. Figure 30 shows the residual isochoric heat capacity (top) and the speed of sound (bottom), which were monitored during the development of the present EOS. The isochoric heat capacity shows expected behavior, e.g., the increasing heat capacity of the liquid phase extrapolated to low temperatures, the steep increase of the saturated liquid and vapor lines, which meet in a maximum at the critical temperature, and a continuous positive slope and curvature of the saturated vapor line with increasing temperature. The saturated liquid and vapor lines of the speed of sound reach a minimum at the critical temperature, which is related to the maximum of the isochoric heat capacity. Another noticeable trend is a weak positive curvature of the liquid-phase speed of sound extrapolated to low temperatures ($\partial w/\partial T > 0$), which indicates reasonable extrapolation behavior of the EOS.⁴³ In Fig. 31, temperature as a function of density is shown. Here, it is important that no unreasonable bumps occur in the saturation curves or isobars, and that isobars do not cross each other. Furthermore, the nonlinearity of the rectilinear diameter was minimized as discussed above.

The characteristic ideal curves can be used to assess correct behavior of the equation of state for very high temperatures,

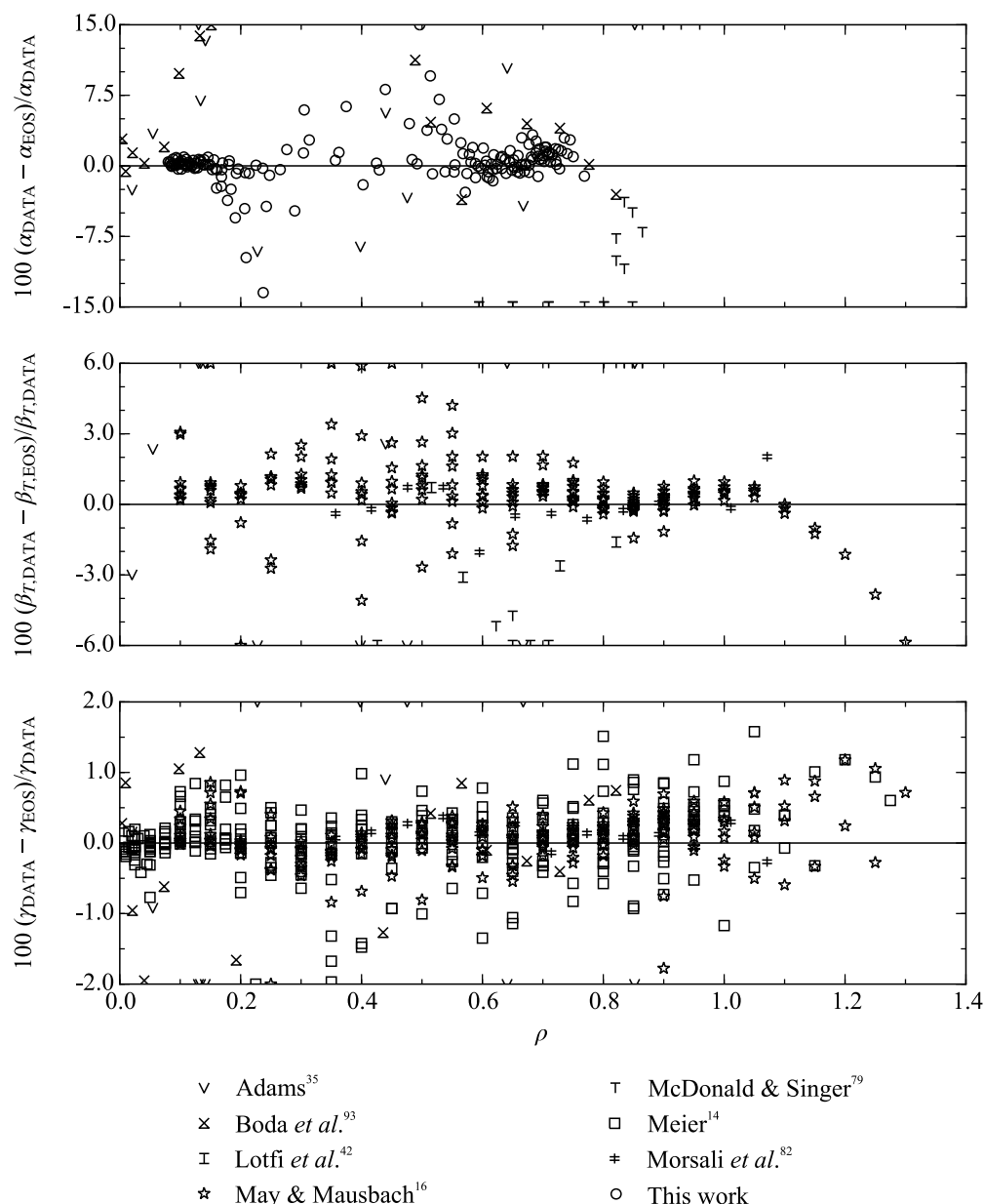


FIG. 29. Relative deviation of literature data for thermal expansion coefficient α , isothermal compressibility β_T , and thermal pressure coefficient γ from the present equation of state.

pressures, and densities.¹²² In Fig. 32, the present EOS and that of Mecke *et al.*⁵ are shown. Data for the EOS of Mecke *et al.*⁵ were compiled with the ThermoC software.^{123,124} Additionally, molecular simulation data^{125–129} are plotted. The two equations agree at the Boyle, ideal, and Joule–Thomson inversion curves, whereas the Joule inversion curves significantly differ from each other. The molecular simulation data indicate that the course of this curve calculated from the equation of Mecke *et al.*⁵ is correct. For all curves, no unphysical bumps or nonmonotonic behavior occurs.

The Grüneisen coefficient as a function of density is shown in Fig. 33. With increasing density, the isotherms should cross each other beyond the critical density. At high temperatures, the Grüneisen coefficient must have a positive slope and negative curvature to ensure correct extrapolation behavior. This is closely related to the bottom plot in Fig. 33, which shows the

Grüneisen coefficient as a function of temperature. This plot looks similar to the speed of sound diagram in Fig. 30. The saturation curves show a steep minimum at the critical temperature. Additionally, isobars for the liquid phase extrapolated to low temperatures are nearly straight lines, with a negative slope. The appropriate course of the Grüneisen coefficient simultaneously ensures correct behavior of the speed of sound, isochoric, and isobaric heat capacity. During the development of the present equation of state, the strategy was found to be much more effective than altering the isochoric heat capacity or the speed of sound directly, which should be taken into consideration in subsequent work.

Another thermodynamic property, established by Venkatarathnam and Oellrich,¹³⁰ is the so-called phase identification parameter Π , originally developed to distinguish between vapor and liquid phases without determining the saturation

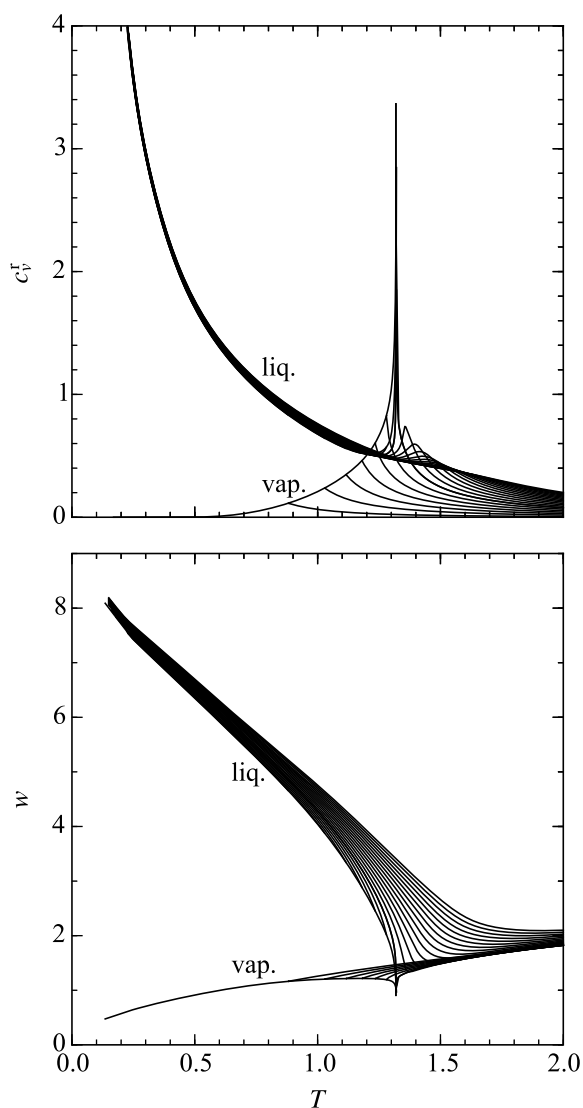


FIG. 30. Top: Residual isochoric heat capacity versus temperature along isobars. Bottom: Speed of sound versus temperature along isobars.

curves. Like the Grüneisen coefficient, this property is not applied for practical purposes. However, in the context of developing equations of state, it may be used to constrain the behavior of EOS correlations. The property is valuable since many different derivatives of the Helmholtz energy are involved (cf. Eq. (26)) and incorrect physical behavior may be detected easily. Figure 34 shows Π along isotherms and isobars. On the top panel, the saturated liquid line shows a negative slope and curvature until the critical density is reached. It exhibits negative slope and positive curvature for increasing density starting at the critical density. Supercritical isotherms form a minimum for $\rho < \rho_c$, cross each other at the critical density, and exhibit a maximum in their further course. Any unreasonable behavior of the EOS can easily be detected. Typical problems, which can occur during the fitting procedure, are multiple oscillations of supercritical isotherms and bumps along the saturated liquid line. These problems would also arise in the bottom panel of Fig. 34, where the phase identification parameter is illustrated as a function of

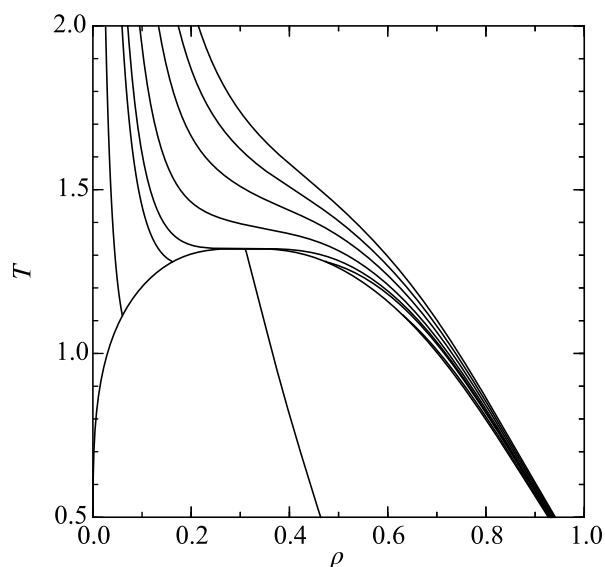


FIG. 31. Temperature versus density along isobars.

temperature along selected isobars. Both saturated liquid and vapor lines have a moderate slope until reaching the vicinity of the critical region. Here, the saturated liquid line increases with distinct positive curvature until it reaches the critical point. In contrast, the saturated vapor line decreases with pronounced negative curvature until reaching the critical point. Supercritical isobars have positive slope and curvature until they reach a maximum at the critical temperature, then they cross each other and converge at high temperatures.

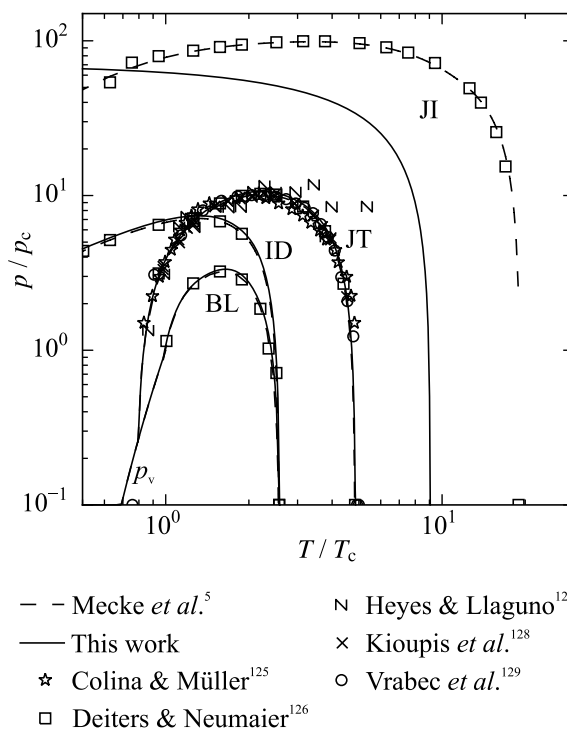


FIG. 32. Characteristic ideal curves as defined by Span and Wagner.¹²² p_v : vapor pressure curve, BL: Boyle curve, ID: ideal curve, JT: Joule-Thomson inversion curve, and JI: Joule inversion curve.

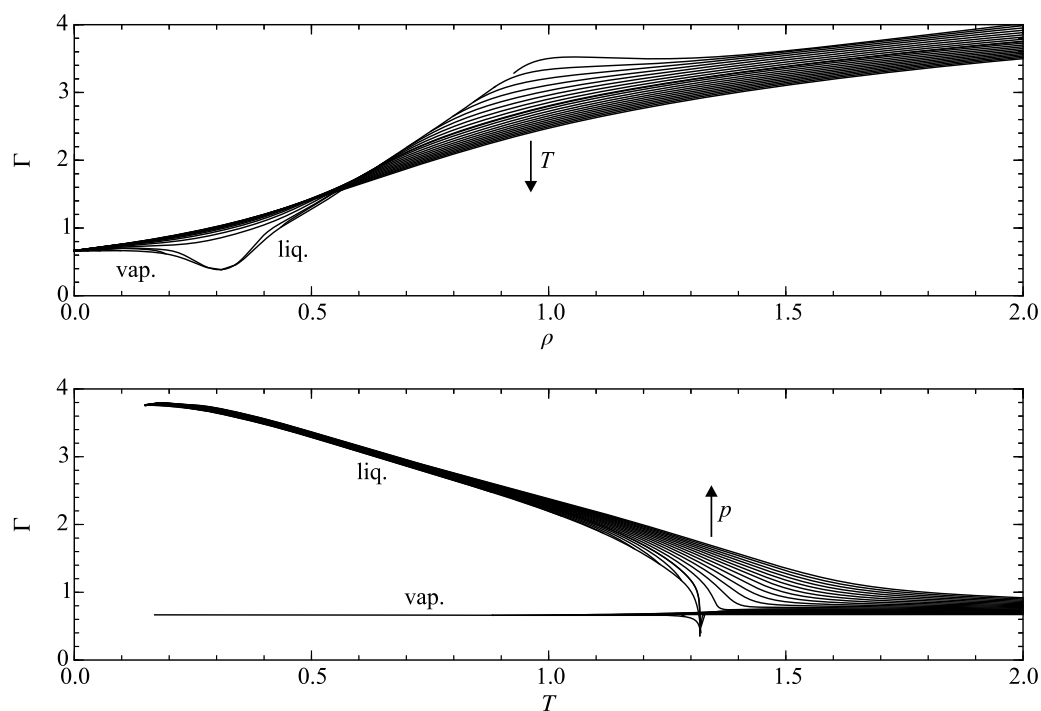


FIG. 33. Gruneisen coefficient versus density along isotherms (top) and Gruneisen coefficient versus temperature (bottom) along isobars.

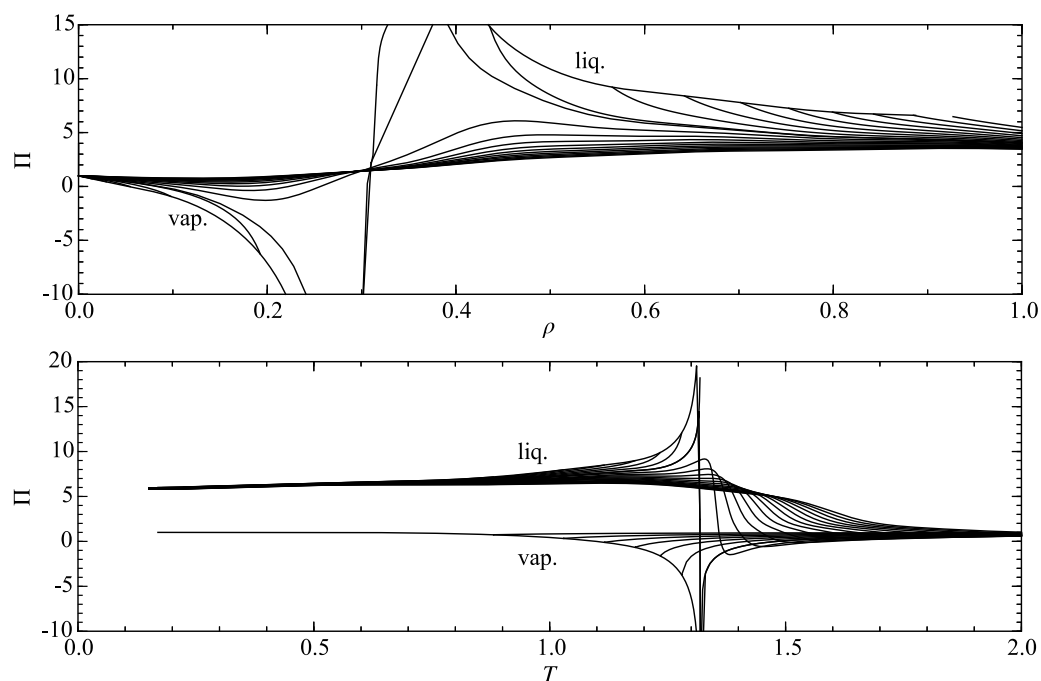


FIG. 34. Phase identification parameter versus density along isotherms (top) and versus temperature along isobars (bottom).

6. Conclusion

The fundamental equation of state developed in this work is explicit in the reduced Helmholtz energy and has an exact ideal-gas contribution. The residual part stems from modern fitting techniques and consists of 23 terms. It is valid for reduced temperatures $0.661 < T < 9$ and for reduced pressures up to $p = 65$, corresponding to $0.5 < T/T_c < 7$ and

$p/p_c = 500$. For its development, only data for residual Helmholtz energy derivatives and virial coefficients were used. Molecular simulation data from the literature and the equation of state of Mecke *et al.*,⁵ which was the best model available in the literature so far, were used to evaluate the present equation comprehensively. The uncertainty of the present EOS is estimated to be 1.8% in vapor pressure and saturated vapor density, and 0.15%–0.5% in saturated liquid density. Uncertainty in

density is 0.1% in the liquid phase, 1% in the gaseous phase, and 0.15%–0.3% in the supercritical region. The uncertainty in pressure amounts to 2% in the critical region. The residual internal energy is reproduced within 1% in the gaseous region, 0.1% in the liquid region, and 1% in the critical and supercritical region. Uncertainty in isochoric heat capacity is 0.5%, whereas the uncertainty in isobaric heat capacity and speed of sound is 1%. The uncertainty of the Grüneisen coefficient is 1.5% and the Joule–Thomson coefficient deviates by 2.5% ($\rho \leq 0.6$) to 10%. The thermal expansion coefficient is reproduced within 15%. The uncertainty of the isothermal compressibility and the thermal pressure coefficient amounts to 3% and 1%, respectively. The overall representation of the simulation data as well as the extrapolation behavior is a significant improvement over existing correlations.

In the supplementary material,⁵² molecular simulation data of this work, a fluid file for the application in the software package TREND,⁴⁴ and a C++ source code are provided. For the verification of computer implementation, reference values for some properties at different state points are also given.

Acknowledgments

This work was part of a comprehensive research program supported by the German Research Foundation (DFG). The simulations were carried out on the national supercomputer hazelhen at the High Performance Computing Center Stuttgart (HLRS) within Project No. MMHBF2.

7. References

- ¹J. E. Jones, *Proc. R. Soc. A* **106**, 441 (1924).
- ²J. E. Jones, *Proc. R. Soc. A* **106**, 463 (1924).
- ³J. K. Johnson, J. A. Zollweg, and K. E. Gubbins, *Mol. Phys.* **78**, 591 (1993).
- ⁴J. Kolafa and I. Nezbeda, *Fluid Phase Equilib.* **100**, 1 (1994).
- ⁵M. Mecke, A. Müller, J. Winkelmann, J. Vrabec, J. Fischer, R. Span, and W. Wagner, *Int. J. Thermophys.* **17**, 391 (1996); Erratum **19**, 1493 (1998).
- ⁶G. Rutkai, M. Thol, R. Lustig, R. Span, and J. Vrabec, *J. Chem. Phys.* **139**, 041102 (2013).
- ⁷R. Lustig, *J. Chem. Phys.* **100**, 3060 (1994).
- ⁸R. Lustig, *J. Chem. Phys.* **100**, 3068 (1994).
- ⁹R. Lustig, *J. Chem. Phys.* **100**, 3048 (1994).
- ¹⁰R. Lustig, *J. Chem. Phys.* **109**, 8816 (1998).
- ¹¹R. Lustig, *Ber. Bunsen-Ges. Phys. Chem.* **98**, 706 (1994).
- ¹²R. Lustig, *Ber. Bunsen-Ges. Phys. Chem.* **99**, 1462 (1995).
- ¹³A. Friedrich and R. Lustig, *J. Mol. Liq.* **98–99**, 243 (2002).
- ¹⁴K. Meier, Ph.D. thesis, University of the Federal Armed Forces Hamburg, 2002.
- ¹⁵K. Meier and S. Kabelac, *J. Chem. Phys.* **124**, 064104 (2006).
- ¹⁶H.-O. May and P. Mausbach, *AIP Conf. Proc.* **1501**, 954 (2012).
- ¹⁷R. Lustig, *Mol. Simul.* **37**, 457 (2011).
- ¹⁸R. Lustig, *Mol. Phys.* **110**, 3041 (2012).
- ¹⁹C. W. Glass, S. Reiser, G. Rutkai, S. Deublein, A. Köster, G. Guevara-Carrion, A. Wafai, M. Horsch, M. Bernreuther, and T. Windmann, *Comput. Phys. Commun.* **185**, 3302 (2014).
- ²⁰B. Widom, *J. Chem. Phys.* **39**, 2808 (1963).
- ²¹M. P. Allen and D. J. Tildesley, *Computer Simulation of Liquids* (Clarendon Press, Oxford, 1987).
- ²²D. Levesque and L. Verlet, *Phys. Rev.* **182**, 307 (1969).
- ²³I. R. McDonald and K. Singer, *Mol. Phys.* **23**, 29 (1972).
- ²⁴Y. Song and E. A. Mason, *J. Chem. Phys.* **91**, 7840 (1989).
- ²⁵J. J. Nicolas, K. E. Gubbins, W. B. Streett, and D. J. Tildesley, *Mol. Phys.* **37**, 1429 (1979).
- ²⁶Y. Adachi, I. Fijihara, M. Takamiya, and K. Nakanishi, *Fluid Phase Equilib.* **39**, 1 (1988).
- ²⁷Y. Miyano, *Fluid Phase Equilib.* **85**, 71 (1993).
- ²⁸R. Span, *Multiparameter Equations of State: An Accurate Source of Thermodynamic Property Data* (Springer, Berlin, 2000).
- ²⁹J. A. Barker, P. J. Leonard, and A. Pompe, *J. Chem. Phys.* **44**, 4206 (1966).
- ³⁰H.-O. May and P. Mausbach, *Phys. Rev. E* **85**, 031201 (2012); Erratum **86**, 059905 (2012).
- ³¹U. Setzmann and W. Wagner, *Int. J. Thermophys.* **10**, 1103 (1989).
- ³²J. P. Valleau (personal communication to Mecke *et al.*, 1996).
- ³³R. J. Wheatley (personal communication, 2013).
- ³⁴A. Ahmed and R. J. Sadus, *J. Chem. Phys.* **131**, 174504 (2009); Erratum **133**, 229902 (2010).
- ³⁵D. J. Adams, *Mol. Phys.* **29**, 307 (1975).
- ³⁶D. J. Adams, *Mol. Phys.* **32**, 647 (1976).
- ³⁷J.-P. Hansen, *Phys. Rev. A* **2**, 221 (1970).
- ³⁸J.-P. Hansen and L. Verlet, *Phys. Rev.* **184**, 151 (1969).
- ³⁹J. Kolafa, H. L. Vörtlér, K. Aim, and I. Nezbeda, *Mol. Simul.* **11**, 305 (1993).
- ⁴⁰B. Saager and J. Fischer, *Fluid Phase Equilib.* **57**, 35 (1990).
- ⁴¹L. Verlet, *Phys. Rev.* **159**, 98 (1967).
- ⁴²A. Lotfi, J. Vrabec, and J. Fischer, *Mol. Phys.* **76**, 1319 (1992).
- ⁴³E. W. Lemmon, M. O. McLinden, and W. Wagner, *J. Chem. Eng. Data* **54**, 3141 (2009).
- ⁴⁴R. Span, T. Eckermann, S. Herrig, S. Hielscher, and M. Thol, *TREND. Thermodynamic Reference and Engineering Data 2.0* (Lehrstuhl für Thermodynamik, Ruhr-Universität Bochum, Bochum, Germany, 2015).
- ⁴⁵E. W. Lemmon, M. L. Huber, and M. O. McLinden, *REFPROP. Reference Fluid Thermodynamic and Transport Properties*, Version 9.1 (National Institute of Standards and Technology, Gaithersburg, MD, 2014).
- ⁴⁶I. H. Bell, J. Wronski, S. Quoilin, and V. Lemort, *Ind. Eng. Chem. Res.* **53**, 2498 (2014).
- ⁴⁷M. A. van der Hoef, *J. Chem. Phys.* **113**, 8142 (2000).
- ⁴⁸R. Agrawal and D. A. Kofke, *Mol. Phys.* **85**, 43 (1995).
- ⁴⁹J. R. Errington, *J. Chem. Phys.* **120**, 3130 (2004).
- ⁵⁰E. A. Mastny and J. J. de Pablo, *J. Chem. Phys.* **127**, 104504 (2007).
- ⁵¹A. Ladd and L. V. Woodcock, *Chem. Phys. Lett.* **51**, 155 (1977).
- ⁵²See supplementary material at <http://dx.doi.org/10.1063/1.4945000> for numerical test values for the verification of computer implementation, comparisons of the present equation of state with simulated reduced Helmholtz derivatives and residual enthalpies, numerical values of the simulation data generated for this work, the fluid file for the calculation of thermodynamic properties the Lennard-Jones model fluid with Trend,⁴⁴ and the C++ source code for the calculation of homogeneous thermodynamic properties of the Lennard-Jones model fluid.
- ⁵³K. R. S. Shaul, A. J. Schultz, and D. A. Kofke, *Collect. Czech. Chem. Commun.* **75**, 447 (2010).
- ⁵⁴R. B. Bird, E. L. Spotz, and J. O. Hirschfelder, *J. Chem. Phys.* **18**, 1395 (1950).
- ⁵⁵J. O. Hirschfelder, C. F. Curtiss, and R. B. Bird, *Molecular Theory of Gases and Liquids* (Wiley, New York, 1954).
- ⁵⁶T. Sun and A. S. Teja, *J. Phys. Chem.* **100**, 17365 (1996).
- ⁵⁷A. Friedrich and R. Lustig, *J. Chem. Phys.* **105**, 9597 (1996).
- ⁵⁸T. Breitenstein and R. Lustig, *J. Mol. Liq.* **98–99**, 263 (2002).
- ⁵⁹T. Breitenstein, Ph.D. thesis, RWTH Aachen, 2000.
- ⁶⁰C. Tegeler, R. Span, and W. Wagner, *J. Phys. Chem. Ref. Data* **28**, 779 (1999).
- ⁶¹R. Gilgen, R. Kleinrahm, and W. Wagner, *J. Chem. Thermodyn.* **26**, 383 (1994).
- ⁶²M. Thol, G. Rutkai, R. Span, J. Vrabec, and R. Lustig, *Int. J. Thermophys.* **36**, 25 (2015).
- ⁶³D. J. Adams, *Mol. Phys.* **37**, 211 (1979).
- ⁶⁴D. A. Kofke, *J. Chem. Phys.* **98**, 4149 (1993).
- ⁶⁵B. Smit and D. Frenkel, *Mol. Phys.* **68**, 951 (1989).
- ⁶⁶A. Z. Panagiotopoulos, *Mol. Phys.* **61**, 813 (1987).
- ⁶⁷A. Z. Panagiotopoulos, N. Quirke, M. Stapleton, and D. J. Tildesley, *Mol. Phys.* **63**, 527 (1988).
- ⁶⁸Because one of the present authors has co-authored Ref. 42, we would like to point out that the employed simulation tool is completely independent of what we have used in the 1990s.
- ⁶⁹M. G. Martin and J. I. Siepmann, *J. Phys. Chem. B* **102**, 2569 (1998).
- ⁷⁰J. J. Potoff and A. Z. Panagiotopoulos, *J. Chem. Phys.* **112**, 6411 (2000).

- ⁷¹W. Shi and J. K. Johnson, *Fluid Phase Equilib.* **187–188**, 171 (2001).
- ⁷²J. E. Hunter and W. P. Reinhardt, *J. Chem. Phys.* **103**, 8627 (1995).
- ⁷³V. G. Baidakov, G. G. Chernykh, and S. Protsenko, *Chem. Phys. Lett.* **321**, 315 (2000).
- ⁷⁴M. Mecke, J. Winkelmann, and J. Fischer, *J. Chem. Phys.* **107**, 9264 (1997).
- ⁷⁵R. Lustig, G. Rutkai, and J. Vrabec, *Mol. Phys.* **113**, 910 (2015).
- ⁷⁶D. D. Carley, *J. Chem. Phys.* **67**, 4812 (1977).
- ⁷⁷W. Fickett and W. W. Wood, *Phys. Fluids* **3**, 204 (1960).
- ⁷⁸I. R. McDonald and K. Singer, *J. Chem. Phys.* **50**, 2308 (1969).
- ⁷⁹I. R. McDonald and K. Singer, *Discuss. Faraday Soc.* **43**, 40 (1967).
- ⁸⁰I. R. McDonald and K. Singer, *J. Chem. Phys.* **47**, 4766 (1967).
- ⁸¹I. R. McDonald and L. V. Woodcock, *J. Phys. C: Solid State Phys.* **3**, 722 (1970).
- ⁸²A. Morsali, S. A. Beyramabadi, and M. R. Bozorgmehr, *Chem. Phys.* **335**, 194 (2007).
- ⁸³F. H. Ree, *J. Chem. Phys.* **73**, 5401 (1980).
- ⁸⁴P. Schofield, *Comput. Phys. Commun.* **5**, 17 (1973).
- ⁸⁵M. S. Shaw, *J. Chem. Phys.* **89**, 2312 (1988).
- ⁸⁶G. M. Sowers and S. I. Sandler, *Fluid Phase Equilib.* **67**, 127 (1991).
- ⁸⁷W. B. Streett, H. J. Raveché, and R. D. Mountain, *J. Chem. Phys.* **61**, 1960 (1974).
- ⁸⁸S. Toxvaerd and E. Praetgaard, *J. Chem. Phys.* **53**, 2389 (1970).
- ⁸⁹L. Verlet and D. Levesque, *Physica* **36**, 254 (1967).
- ⁹⁰J. D. Weeks, D. Chandler, and H. C. Andersen, *J. Chem. Phys.* **55**, 5422 (1971).
- ⁹¹W. W. Wood, in *Physics of Simple Liquids*, edited by H. N. V. Temperley, J. S. Rowlinson, and G. S. Rushbrooke (North Holland Publishing Company, Amsterdam, 1968), pp. 115–230.
- ⁹²W. W. Wood and F. R. Parker, *J. Chem. Phys.* **27**, 720 (1957).
- ⁹³D. Boda, T. Lukács, J. Liszi, and I. Szalai, *Fluid Phase Equilib.* **119**, 1 (1996).
- ⁹⁴I. Szalai, J. Liszi, and J. Fischer (private communication to Mecke *et al.*, 1994).
- ⁹⁵J. S. Emampour, A. Morsali, S. A. Beyramabadi, M. R. Bozorgmehr, and K. Khakzadan, *Int. J. Phys. Sci.* **6**, 5731 (2011).
- ⁹⁶P. Mausbach and H.-O. May, *Fluid Phase Equilib.* **366**, 108 (2014).
- ⁹⁷R. Span and W. Wagner, *J. Phys. Chem. Ref. Data* **25**, 1509 (1996).
- ⁹⁸R. Span, E. W. Lemmon, R. T. Jacobsen, W. Wagner, and A. Yokozeki, *J. Phys. Chem. Ref. Data* **29**, 1361 (2000).
- ⁹⁹J. A. Zollweg and G. W. Mulholland, *J. Chem. Phys.* **57**, 1021 (1972).
- ¹⁰⁰A. Linhart, C.-C. Chen, J. Vrabec, and H. Hasse, *J. Chem. Phys.* **122**, 144506 (2005).
- ¹⁰¹D. O. Dunikov, S. P. Malysenko, and V. V. Zhakhovskii, *J. Chem. Phys.* **115**, 6623 (2001).
- ¹⁰²J. M. Caillol, *J. Chem. Phys.* **109**, 4885 (1998).
- ¹⁰³S. Hess, *Physica A* **267**, 58 (1999).
- ¹⁰⁴J. J. Potoff and A. Z. Panagiotopoulos, *J. Chem. Phys.* **109**, 10914 (1998).
- ¹⁰⁵B. Smit, *J. Chem. Phys.* **96**, 8639 (1992).
- ¹⁰⁶S. H. Sung and D. Chandler, *Phys. Rev. A* **9**, 1688 (1974).
- ¹⁰⁷D. J. Adams, E. M. Adams, and G. J. Hills, *Mol. Phys.* **38**, 387 (1979).
- ¹⁰⁸A. Amadei, G. Apol, G. Chillemi, H. J. C. Berendsen, and A. Di Nola, *Mol. Phys.* **96**, 1469 (1999).
- ¹⁰⁹S. Kim, D. Henderson, and J. A. Barker, *Can. J. Phys.* **47**, 99 (1969).
- ¹¹⁰D. A. Kofke, *Mol. Phys.* **78**, 1331 (1993).
- ¹¹¹N. K. Koutras, V. I. Harismiadis, and D. P. Tassios, *Fluid Phase Equilib.* **77**, 13 (1992).
- ¹¹²J. Sýs and A. Malijevský, *Collect. Czech. Chem. Commun.* **45**, 977 (1980).
- ¹¹³V. Arp, J. M. Persichetti, and G.-b. Chen, *J. Fluids Eng.* **106**, 193 (1984).
- ¹¹⁴M. Thol, G. Rutkai, A. Köster, M. Kortmann, R. Span, and J. Vrabec, *Chem. Eng. Sci.* **121**, 87 (2015); Erratum **134**, 887 (2015).
- ¹¹⁵M. Thol, F. Dubberke, G. Rutkai, T. Windmann, A. Köster, R. Span, and J. Vrabec, *Fluid Phase Equilib.* **418**, 133 (2016).
- ¹¹⁶M. Thol and E. W. Lemmon, *Int. J. Thermophys.* **37**, 28 (2016).
- ¹¹⁷R. Akasaka, Y. Zhou, and E. W. Lemmon, *J. Phys. Chem. Ref. Data* **44**, 013104 (2015).
- ¹¹⁸H. Gedanitz, M. J. Davila, and E. W. Lemmon, *J. Chem. Eng. Data* **60**, 1331 (2015).
- ¹¹⁹Y. Zhou, J. Liu, S. G. Penoncello, and E. W. Lemmon, *J. Phys. Chem. Ref. Data* **43**, 043105 (2014).
- ¹²⁰M. Thol, E. W. Lemmon, and R. Span, *High Temp. - High Pressures* **41**, 81 (2012).
- ¹²¹W. Wagner and M. Thol, *J. Phys. Chem. Ref. Data* **44**, 043102 (2015).
- ¹²²R. Span and W. Wagner, *Int. J. Thermophys.* **18**, 1415 (1997).
- ¹²³U. K. Deiters, ThermoC software, University of Cologne, <http://thermoc.uni-koeln.de/index.html> (accessed March 9, 2016).
- ¹²⁴U. K. Deiters, *Chem. Eng. Technol.* **23**, 581 (2000).
- ¹²⁵C. M. Colina and E. A. Müller, *Int. J. Thermophys.* **20**, 229 (1999).
- ¹²⁶U. K. Deiters and A. Neumaier, “Computer simulation of the characteristic curves of pure fluids,” *J. Chem. Eng. Data* (in press).
- ¹²⁷D. M. Heyes and C. T. Llaguno, *Chem. Phys.* **168**, 61 (1992).
- ¹²⁸L. I. Kioupis, G. Arya, and E. J. Maginn, *Fluid Phase Equilib.* **200**, 93 (2002).
- ¹²⁹J. Vrabec, G. K. Kedia, and H. Hasse, *Cryogenics* **45**, 253 (2005).
- ¹³⁰G. Venkatarathnam and L. Oellrich, *Fluid Phase Equilib.* **301**, 225 (2011).